University of South Bohemia

Faculty of Science

Light harvesting complexes and chromatic adaptation of Eustigmatophyte alga *Trachydiscus minutus*

Master thesis

Bc. Marek Pazderník

Instructor: RNDr. Radek Litvín, Ph.D.

České Budějovice 2015

Pazderník, M., 2015: Light harvesting complexes and chromatic adaptation of Eustigmatophyte alga *Trachydiscus minutus.* Mgr. Thesis, in English. – 53 p., Faculty of Science, University of South Bohemia, České Budějovice, Czech Republic.

Annotation:

The chromatic adaptation of *Trachydiscus minutus* was investigated by separation of light harvesting complexes (antennae and photosystems) on a sucrose gradient using variety of detergents and their concentrations, further complex purification and characterization was done using biochemical separation and spectroscopic techniques.

Prohlašuji, že svoji diplomovou práci jsem vypracoval samostatně pouze s použitím pramenů a literatury uvedených v seznamu citované literatury.

Prohlašuji, že v souladu s § 47b zákona č. 111/1998 Sb. v platném znění souhlasím se zveřejněním své diplomové práce, a to v nezkrácené podobě elektronickou cestou ve veřejně přístupné části databáze STAG provozované Jihočeskou univerzitou v Českých Budějovicích na jejích internetových stránkách, a to se zachováním mého autorského práva k odevzdanému textu této kvalifikační práce. Souhlasím dále s tím, aby toutéž elektronickou cestou byly v souladu s uvedeným ustanovením zákona č. 111/1998 Sb. zveřejněny posudky školitele a oponentů práce i záznam o průběhu a výsledku obhajoby kvalifikační práce. Rovněž souhlasím s porovnáním textu mé kvalifikační práce s databází kvalifikačních prací Theses.cz provozovanou Národním registrem vysokoškolských kvalifikačních prací a systémem na odhalování plagiátů.

České Budějovice, 21. 03. 2015
Podpis:

Contents:

Goals of the thesis:

1. **Optimization of the method used for isolation of light harvesting complexes from *T. minutus*.**

- Finding a detergent type and concentration suitable for sucrose gradient separation.

2. **Investigation of the light harvesting complex composition of *T. minutus* grown under red light conditions.**

- Elucidation of the molecular mechanism responsible for the shift in the absorption and fluorescence emission

List of used abbreviations:

ADP – Adenosine diphosphate

ATP – Adenosine triphosphate

ATPase – ATP synthase

Chl - Chlorophyll

CN – Clean native electrophoresis

FCP – Fucoxanthin-Chlorophyll protein

HL – High light

HOMO – Highest occupied molecular orbital

LHC – Light harvesting complex

LL – Low light

LUMO – Lowest unoccupied molecular orbital

NADPH – Nicotinamide adenine dinucleotide phosphate

Pi – Phosphate

PSI – Photosystem I

PSII – Photosystem II

RC – Reaction center

RL – Red light

SDS-PAGE – Sodium dodecyl sulfate polyacrylamide gel electrophoresis

VCP – Violaxanthin-Chl protein

α-DM – n-dodecyl α-D-maltoside

β-DM – n-dodecyl β-D-maltoside

1. Introduction

1.1 Principles of photosynthesis in eukaryotes

1.1.1 Function and structure of photosynthetic pigments

Photosynthesis is a process of transforming energy carried by photons into energy stored in chemical bonds. This process will be briefly described in following chapters. Initial step in photosynthesis is a photon absorption by a pigment. Pigments are molecules which absorb certain range of visible light, giving a color to the material which contains them. The energy of absorbed photon is transformed into energy of an electronic excited state. This energy of excited electron is then further used as described in section 1.1.2. Eukaryotic photosynthetic organisms use two types of pigments for light absorption: chlorophylls and carotenoids.

Chlorophylls serve as the major light absorbing molecules across all photosynthetic life. All chlorophylls have a system of conjugated double bonds (figure 1). These delocalized π-electrons are responsible for absorption of visible light. They form the highest occupied molecular orbitals (HOMOs) of the molecule, from which the electrons are excited to nonbonding and antibonding molecular orbitals (LUMOs) while absorbing photons. With the increasing number of conjugated double bonds the energy gap between HOMOs and LUMOs gets smaller, resulting in possible absorption of less energetic light.

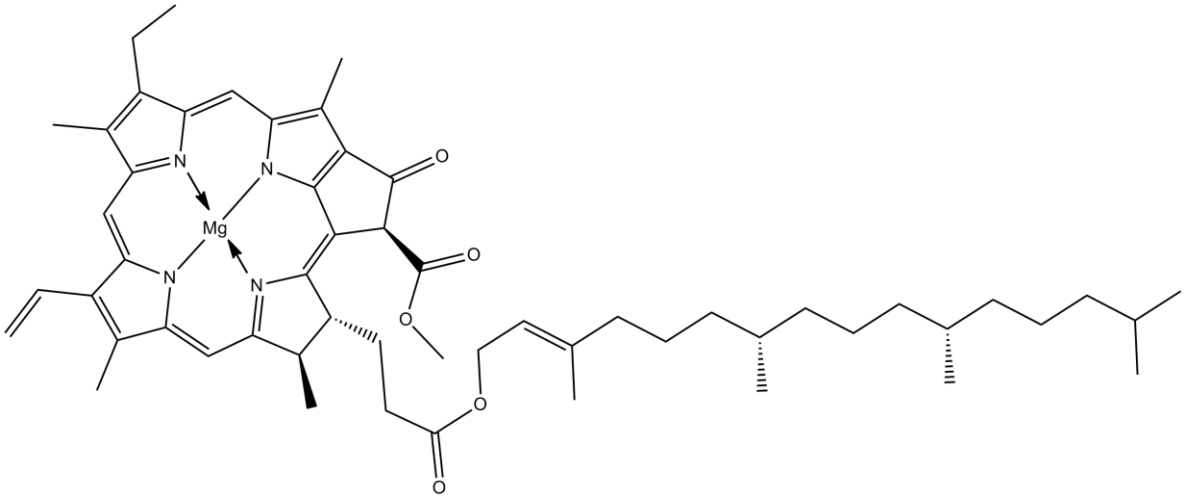

Fig. 1. Structure of chlorophyll a.

Chlorophylls absorb visible light mainly in two wavelength ranges (figure 2), the lower energy absorption bands (600-700 nm) correspond to electron excitation to S_1 region (in the

case of chlorophylls called Q states) and higher energy absorption bands (400-500 nm) corresponds to transitions to S_2 region (called B states or Soret states) (Blankenship 2014).

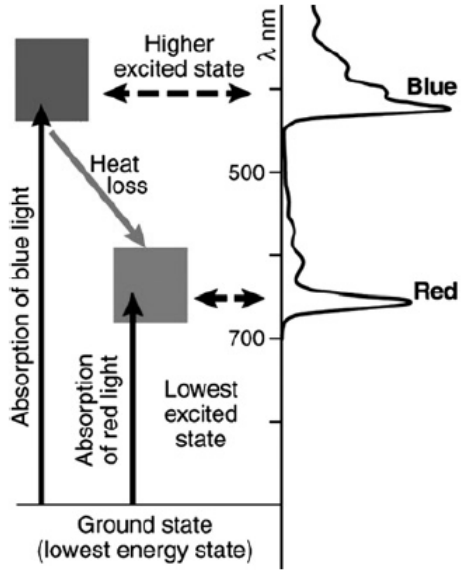

Fig. 2. Absorption spectrum and simplified energy level diagram of chlorophyll *a* (Blankenship 2014).

Carotenoid pigments along with chlorophylls form the available pool of pigments in eukaryotic photosynthesis. Also, carotenoids are present in all known photosynthetic organisms (Polivka and Frank 2010). Hundreds of variants of carotenoids are used by various photosynthetic life forms, but they all share delocalized π-electron system, which enables them to absorb light in the visible spectrum, similarly to chlorophylls. They are divided into two groups: carotenes and xantophylls. They both share the basic carotenoid skeleton made by the mevalonate pathway, however xantophylls contain oxygen atoms, carotenes do not (figure 3). Several functions are assigned to carotenoids in photosynthesis. They serve as accessory collectors of energy from light, mainly in the region where chlorophylls do not absorb (500-600 nm). Carotenoids also contribute to the protection of the photosynthetic apparatus from energy overload. Excess of excitation energy on chlorophylls can lead to formation of so called reactive oxygen species, which are highly reactive and can cause damaging changes to other molecules. Rate of the formation of reactive oxygen species is slowed down by transferring the energy excess from chlorophylls onto carotenoids. (Blankenship 2014).

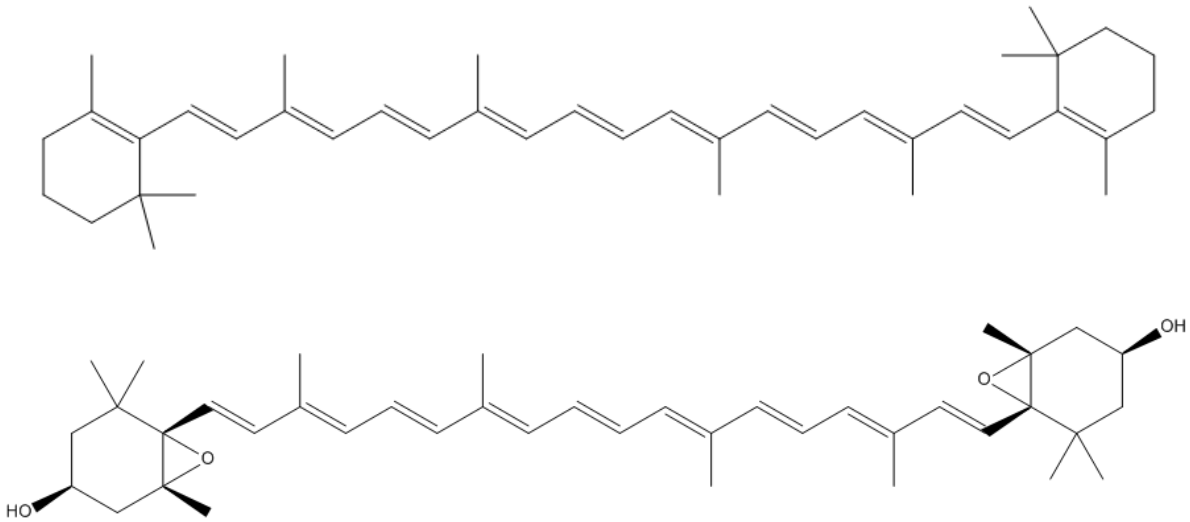

Fig. 3. Structures of β-carotene (up) and violaxanthin (down), as representatives of carotenoids and xantophylls in the studied alga *T. minutus*.

The energy of an excited pigment can transfer itself onto another pigment molecule (as mentioned above) before it is dissipated as heat or fluorescence, only if the "acceptor" pigment is in correct distance and orientation from the "donor". This energy transfer is used in photosynthesis to a great extent. To keep the pigments in the desired conformation, they are held together by proteins. The energy transfer between pigments is today explained by three theories. Förster theory of energy transfer (Förster 1965), exciton coupling (van Armerongen *et al*. 2000) and electronic quantum coherence effects (Scholes 2010).

1.1.2 Light-dependent phase of photosynthesis

The synthesis of saccharides from CO_2 and H_20 in photosynthetic eukaryotes is often divided into two phases. The so called light-dependent phase is the creation of NADPH (from NADP+ and electrons plus proton originating from water) and ATP (from ADP and Pi) using the energy of photons as the initial energy source. It is called light dependent phase because it directly requires photons, in eukaryotes it takes place in and around the most inner chloroplast membrane (called thylakoid membrane). Chloroplast is a specialized photosynthetic organelle in eukaryotes. The thylakoid membrane encloses space which is called thylakoid lumen. The space in between thylakoid membrane and inner chloroplast membrane is called stroma. The light-dependent phase will now be described in the direction of electron flow from water to NADPH. (Schematic representation of this light dependent phase is depicted in figure 5).

So called reaction centers play a central role in the energy transformation during light dependent-phase. Photosynthetic reaction centers are made of proteins, pigments and other co-factors. Each reaction center monomer contains two central chlorophyll molecules (called the “special pair”), which are in tightly held conformation and distance from other pigments. When the special pair gets excited, either by light absorption or transfer of excitation energy from other pigments (as explained in section 1.1.1), so called charge separation takes place (figure 4). Compared to the energy transfer between pigments, charge separation is a process, where the excited electron leaves the excited molecule, leaving it with positive charge, and migrates onto suitable electron acceptor. Therefore these reaction centers transform the energy of electronic excited state into a redox potential. Requirement for this energy transformation is that the molecule which provides the electron (electron donor) has lower redox potential than the electron acceptor.

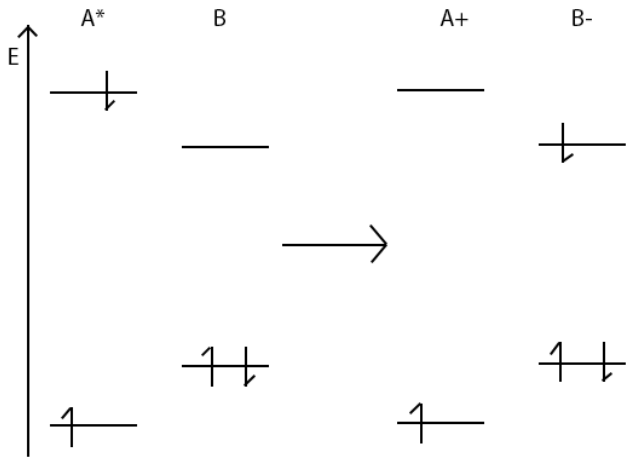

Fig. 4. Charge separation diagram, of excited molecule A (el. donor) and molecule B (el. acceptor).

Eukaryotic organisms have two types of reaction centers. RCI in photosystem I and RCII in photosystem II, they are membrane bound complexes in thylakoid membranes. Also, all photosynthetic eukaryotes share the organization of electron flow from water to ferredoxin, eventually to NADP+. The organization of electron/proton flow during light dependent phase, and chemical balance for creation of one oxygen molecule is depicted on figure 5.

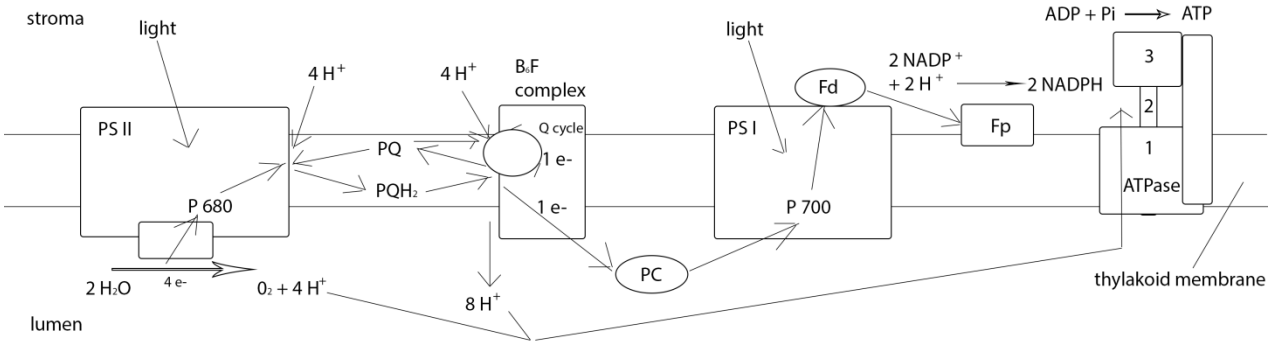

Fig. 5. Electron and proton flow through thylakoid membrane during light dependent phase in eukaryotic chloroplasts.

Photosystem II is the initial complex, where water gets oxidized to molecular oxygen, on so called oxygen evolving complex, which is attached to the core of PSII (Umena *et al.* 2011). Protons are released inside the lumen and electrons pass through the PSII to reduce a plastoquinone to plastoquinole (figure 6). This chemistry is driven by charge separation on chlorophyll special pair P680 with resulting redox potential of +1.2 V. PSII forms a dimeric supercomplex in the thylakoid membrane with so far over 20 identified polypeptide components, variety of pigments and cofactors. The final composition of PSII is species dependent. However the dimeric core which is made of four polypeptides (39 kDa PSII-A/D, 56 kDa PSII-B and 51 kDa PSII-C) and the oxygen evolving complex are preserved (Vinyard *et al*. 2013).

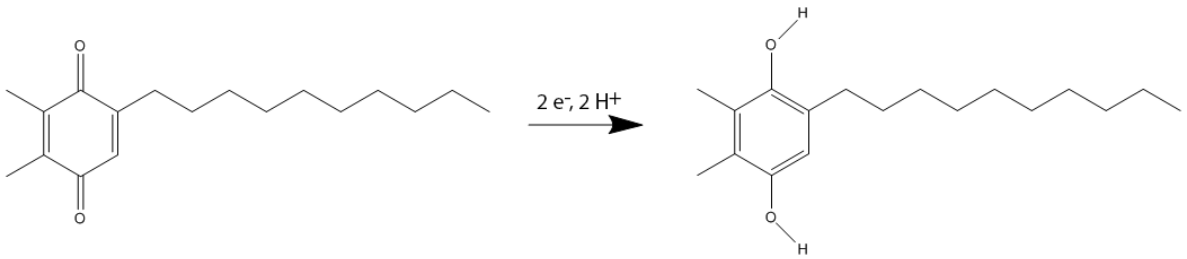

Fig. 6. Two electron reduction of plastoquinone (PQ) to plastoquinol (PQH_2).

Plastoquinone is a two electron carrier. It is a rather hydrophobic molecule which allows it to freely diffuse through the thylakoid membrane. When it gets reduced it takes the two protons from the stroma. On the other hand after oxidation on the b_6f complex it releases those two protons to the lumen side of thylakoid membrane (figure 5 shows 8 protons released into lumen, because for every one oxygen molecule formed 4 plastoquinols get oxidized. Along

with protons released from water, they form a proton gradient across the thylakoid membrane, which is used for ATP synthesis (as described later in this chapter).

Cytochrome b_6f complex (second complex from left, figure 5) mediates the transport of electrons from the "product of PSII" (plastoquinol) to the "reagent of photosystem I" (plastocyanin) (Baniulis *et al*. 2008). Another function of this complex is the transport of protons to the lumen side of thylakoid via the so called Q cycle (Hasan *et al*. 2013).The Q cycle is a repeated reduction of a plastoquinone by electrons from b_6f complex, which is accompanied by intake of protons from the stroma and subsequent release into lumen (figure 5).

Plastocyanin (PC in figure 5) is a copper containing protein and acts as one electron carrier, which transports one electron from the b_6f complex to PSI. Photosystem I has similar function to PSII. Its core is formed by two 82 (PSI-A) and 83 kDa (PSI-B) polypeptides supporting around 100 chlorophylls and 12-16 carotenoids. Electrons from plastocyanins pass through PSI via chlorophyll special pair P700 (which acts as donor in charge separation), and iron-sulphur clusters onto ferredoxin. Ferredoxin is involved in multiple cellular reactions, one of which is NADPH formation by ferredoxin-NADP reductase (Blankenship 2014), ferredoxin can also get oxidized on the b_6f complex via the Q cycle, resulting in a cyclic electron movement, while creating proton gradient (not shown in figure 5).

The protons released in the lumen by water and plastoquinole oxidation (figure 5) create a membrane potential (pH is lower in the lumen side, than in stromal side). This potential drives the ATP synthesis on a membrane bound ATP-synthase (figure 5, ATPase). ATP synthase mediates reaction between ADP and inorganic phosphate. Energy for this reaction is coming from the rotation of the part 1 and 2 (figure 5) of ATP synthase, caused by proton gradient along the thylakoid membrane (chemiosmotic theory) (Noji *et al*. 1997). ATP gets synthesized in the part 3. Part 3 of the ATP synthase has 3 active sites. Each active site can adapt 3 conformations with affinity either for ATP, ADP + Pi or being empty. Rotation of the part 2 induces conformational change in these active sites in the order of: empty -> ADP + Pi -> ATP, resulting in ATP synthesis.

Eukaryotic photosynthetic organisms have their reaction centers composition rather similar to prokaryotic cyanobacteria, resulting in wide acceptance of the endosymbiotic theory

(Margulis 1993) as the origin of chloroplast in eukaryotes. Glaukophytes, a group of eukaryotic algae, have peptidoglycan layer between inner and outer chloroplast membrane, which further suggests the bacterial origin of chloroplast. All photosynthetic eukaryotes are oxygenic, meaning water is used as electron source for the light dependent phase. Prokaryotes can also utilize other electron sources, for example H_2S and H_2 (Blankenship 2012).

1.1.3 Light-independent phase of photosynthesis

NADPH and ATP produced in the light dependent phase (section 1.1.2) are used for CO_2 assimilation and reduction in the Calvin cycle (also called light-independent phase of photosynthesis). Despite its name it takes place only when light is available, because it needs steady supply of NADPH and ATP, which would quickly get depleted during the absence of light. It takes place in the stroma (between thylakoid and inner chloroplast membranes). The synthesis of 1 molecule of glucose via the Calvin cycle is depicted in figure 7. In total 18 ATP and 12 NADPH are used to make one hexose-phosphate from CO_2. Carbohydrates created by the Calvin cycle are further used to fuel anabolic reactions and ATP driven processes within the photosynthetic organism.

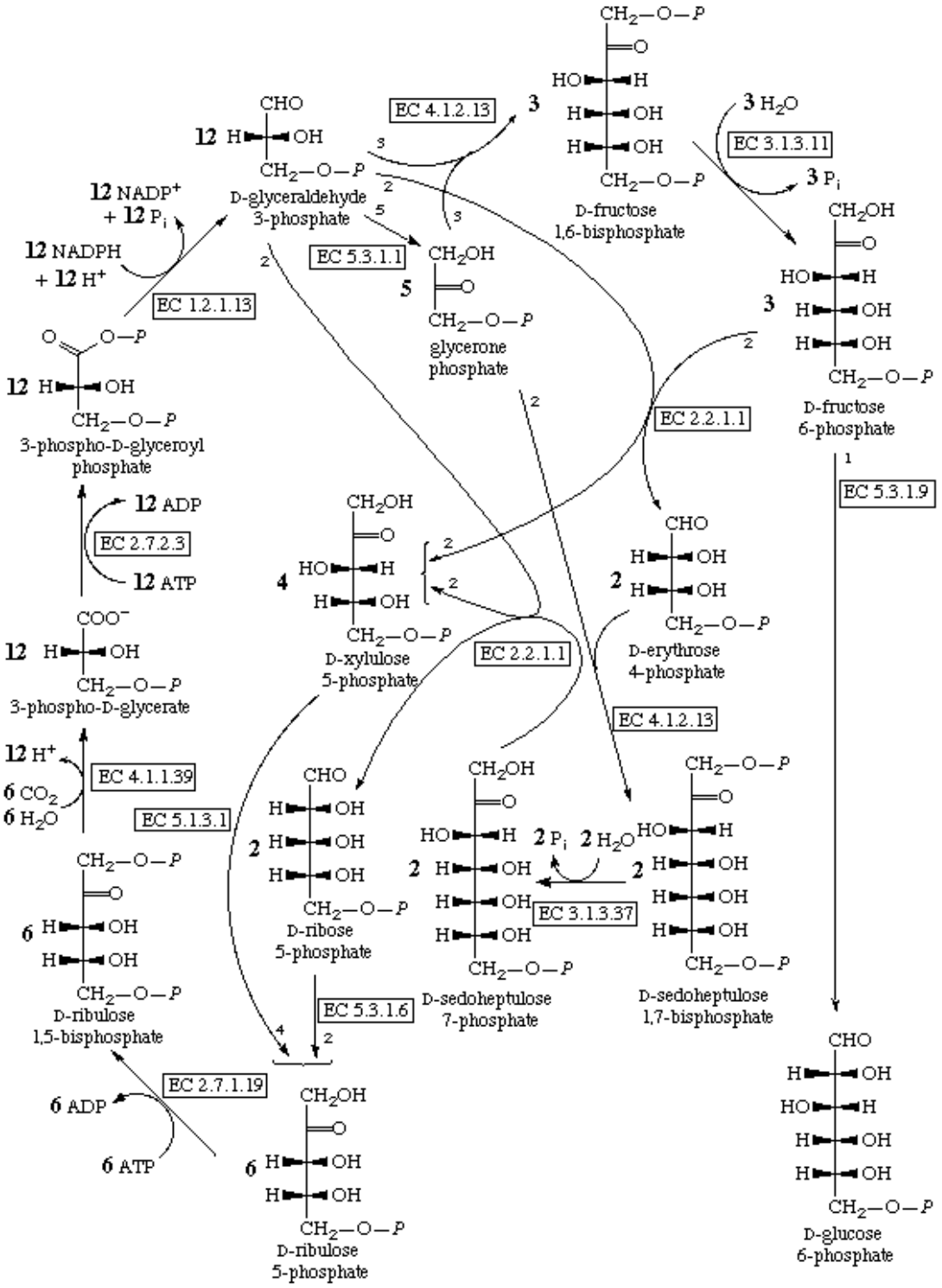

Fig. 7. Synthesis of glucose-6-phosphate from 6 CO_2 via the Calvin cycle [(1)].

1.2 Photosynthetic antennae systems

To regulate the energy available for reaction centers, photosynthetic organisms contain so called antennae systems. The main role of these antenna complexes is to provide more energy for photosynthetic reaction centers. For an effective energy transfer from antenna to RC, antennae need to be in direct contact with a reaction center or with another antenna, which mediates the connection to the RC. Antenna systems consist of very ordered structure of proteins and pigments. The pigments are held together in precise distance and orientation, which is required for an effective energy transfer between them, as previously described in section 1.1.1.

Antennas are divided according to their position within the chloroplast and relation towards reaction center. Inner antennas are constantly fixed near the reaction center. On the other side outer antennas are not permanently attached to the RC, which allows them to mediate the adaptation to environmental changes, by attaching only during certain cellular conditions. Outer antennas can be integral (inside the membrane) and peripheral (outside the membrane) (Blakenship 2014).

1.2.1 Antenna systems in higher plants

The most studied eukaryotic antenna system is light harvesting system II. LHCII monomer (polypeptide sizes around 22-23 kDa, genes encoding these antennas are called Lhcb) is composed of three transmembrane α-helices and one amphiphatic helix, which are in complex with two carotenoid and twelve chlorophyll molecules (Kühlbrandt *et al.* 1994). LHCII monomers can form trimeric structures which connect to PSII core on three possible sites with different affinity (figure 8). Three peripheral monomeric antennas (Lhcb4-6) mediate the connection between LHC II trimers and PSII core. The core of PSII contains two so called inner antenna systems, created by two proteins PSII-C and PSII-B (called CP 43 and CP 47). LHC II can also connect to PSI (Wientjes *et al.* 2013, Allen 1992). LHCII was also reported to form multimeric complexes inside the thylakoid membrane. Dekker *et al.* (1999) reported a complex of seven LHCII trimers.

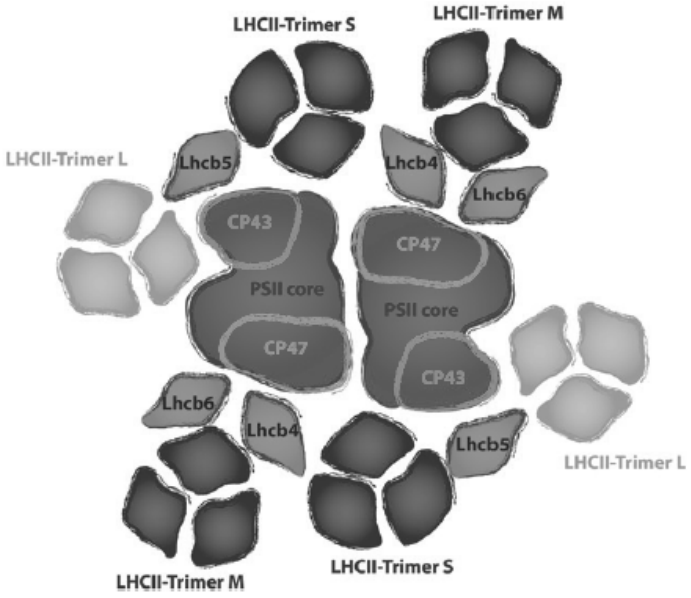

Fig. 8. Organization of PS II with peripheral antennas. The notation S/M/L (strongly/moderately/loosely) describe the relative cohesion of the LHCII-trimer towards the complex. (figure adapted from Ballottari *et al.* 2012)

Photosystem I is in higher plants surrounded from one side by peripheral integral antennas called LHCI. Four distinct genes Lhca1-4 from the LHC gene-superfamily, with protein masses of around 25 kDa, encode these complexes in green plants (fig. 9). (Dekker and Boekema 2005) The reason why the antennas are tightly bound only on one side may be the ability of PSI to form trimers in photosynthetic cyanobacteria, from which eukaryotic photosynthetic apparatus evolved. Photosystem I in the potential PSI trimer would then be accessible for integral antennas only from the side, which is occupied on figure 9.

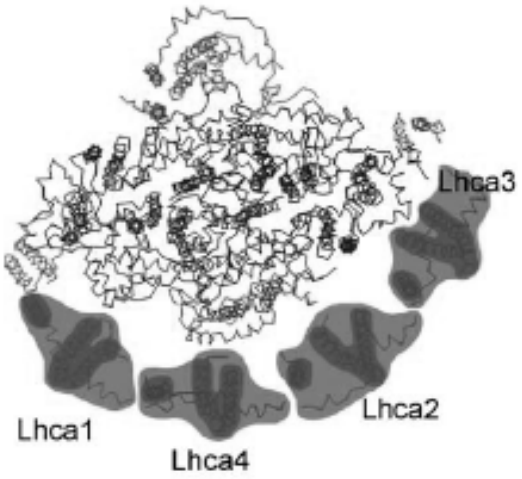

Fig. 9. Structural model of PSI backbone surrounded by four LHCI complexes denoted as Lhca1-4. Figure adapted from (Dekker and Boekema 2005).

1.2.2 Antenna systems of Heterokontophytes

Photosynthetic organisms not directly related to the green plant lineage have similar antenna systems. Diatoms (Bacillariophyceae) a class of algae from the phylum Heterokontophyta were reported to contain so called fucoxanthin–Chl protein antennas (FCP, LHC type antennas named after a dominant pigment fucoxanthin, fig. 10), whose monomeric and oligomeric structures (with protein sizes around 18-19 kDa, Büchel 2003) resemble the LHCII of higher plants. Trimeric antenna complexes which assemble into higher oligomers and are accessory for both photosystems were reported by Lepetit *et al.* (2012) to be widely present across the diatoms.

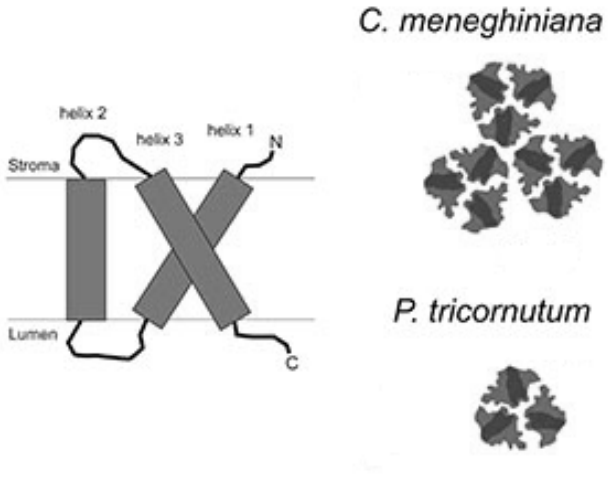

Fig. 10. Schematic representation of FCP monomer backbone (left), oligomeric organization of FCP complexes in two diatoms. A trimer found in *P. tricornutum* and a nonamer found in *C. meneghiniana* (both diatoms). (Figure adapted from Beer *et al.* 2006)

Nannochloropsis gaditana a member of the class Eustigmatophyceae (same as *Trachydiscus minutus*) was also reported to contain LHC type antenna (in this case called VCP after a dominant pigment violaxanthin) by Basso *et al.* (2014), protein sizes of 20-22 kDa were determined to constitute these complexes. This antenna was reported to also form oligomers and to be associated with both photosystems. The main difference of VCP antennas, compared to other members of Heterokonts, was reported to be the lack of other accessory chlorophylls along chlorophyll *a*.

1.3 Eustigmatophyceae and chromatic adaptation

Algae form a large group of eukaryotic photosynthetic organisms (Graham *et al*. 2008). The most studied group are the green algae (chlorophytes, kingdom Archaeplastida), because of their similarity with higher plants. Multiple algal groups belong to a group (kingdom) of protists called Chromalveolata. Their chloroplasts originated in a secondary endosymbiotic event when red algal (Archaeplastida) cell was engulfed by a heterotrophic cell. One of the most important photosynthetic groups of Chromalveolata is phylum Heterokontophyta. The most well-known group of Heterokontophyta are diatoms (class Bacillariophyceae), algae with siliceous cell wall. The Eustigmatophyceae is a class of yellow-green algae also belonging to Heterokonts. The most studied genus of this class is *Nannochloropsis*, because of its potential for light driven biofuel synthesis (Zhang *et al*. 2014, Pedro *et al*. 2014). The most recent overview of the class members was reported by Fawley *at al.* 2014, with presentation of new species. According to the nuclear 18S rDNA sequence, the class consists of two clades Eustigmatales and Goniochloridales, with *T. minutus* assigned to the second one.

Chromatic adaptation is a change in the absorption spectrum of an organism induced by different spectral composition and intensity of incident solar energy. Previously the response to different irradiation levels in eukaryotic marine chlorophyte alga (*Dunaliella tertiolecta*) was studied by Sukenik *et al.* (1988). The reported response was a change in the PSI and PSII abundance, the amount of LHCs attached to the reaction centers, as well as the relative expression of LHCI and LHCII apoproteins. Changes in apoprotein expression can eventually lead to different pigment composition. Recently an antenna complex with 710 nm room temperature fluorescence emission was reported to be responsible for a red light absorption in *Chromera velia* (belongs to a Chromalveolate phylum Chromerida) (Kotabová *et al.* 2014, Bína *et al.* 2014).

1.4 *Trachydiscus minutus*

T. minutus is an eukaryotic photosynthetic unicellular organism belonging to the class of Eustigmatophyceae, under the phylum Heterokontophyta and kingdom Chromalveolata. Closest phylogenetic relative using the 18S rRNA gene sequence is *Goniochloris sculpta* (Přibyl *et al*. 2012). The class contains mostly freshwater species with the only so far known marine genus *Nannochloropsis*.

The studied organism *T. minutus* showed presence of two types of photosynthetic pigments: chlorophylls and carotenoids. The main photosynthetic pigment of *T. minutus* was determined to be chlorophyll *a* (71 %), no other chlorophyll was reported. The remaining 29 % are formed by carotenoids: violaxanthin 56.6 % of total carotenoids, vaucheriaxanthin 25.9 %, β-carotene, zeaxanthin and neoxanthin 9.7 %, 3.2 % and 4.7 % resp. (Přibyl *et al*. 2012).

T. minutus is a candidate for polyunsaturated fatty acids and eicosapentaenoic acid industrial production as reported by Řezanka *et al*. 2010 and Cepák *et al.* 2014. *T. minutus* was the first yellow-green alga reported for production of polyunsaturated triacylglycerols, their production dependence on nitrogen and phosphorus starvation was investigated (Řezanka *et al.* 2011). The effects of different temperatures and light intensities on growth and composition of *T. minutus* were investigated (Gigova *et al.* 2012), the optimal temperature for growth was found to be 25 °C.

2. Materials and methods

Cell growth: Cells were grown on WC medium (Guillard and Lorenzen 1972) under three different light conditions. **High light conditions**: 200 µmol photons.m^{-2}.s^{-1} with spectrum (fig. 11, green), 22 °C, 15 h light/ 9 h dark, light source: HQI-E 250 W/D Pro Daylight. **Low light conditions**: 15 µmol photons.m^{-2}.s^{-1} with spectrum (fig. 11, green), 22 °C, 15 h light/ 9 h dark, light source: HQI-E 250 W/D Pro Daylight. **Red light conditions**: 15 µmol photons.m^{-2}.s^{-1} with spectrum (fig. 11, red), 22 °C, 15 h light/ 9 h dark, light source: tungsten light bulb. Light intensities were measured with Hansatech Quantitherm Light meter (Hansatech Instruments, United Kingdom).

The culture used for growth was 931 *Trachydiscus minutus* (Bourrelly) Ettl obtained as a kind gift of Martin Trtílek. The culture was stirred and filtered air (0.22 µm) was constantly provided during the growth. Cells were collected during late exponential growth phase by centrifugation (4500 g, 5 min) and frozen at -80 °C until further use.

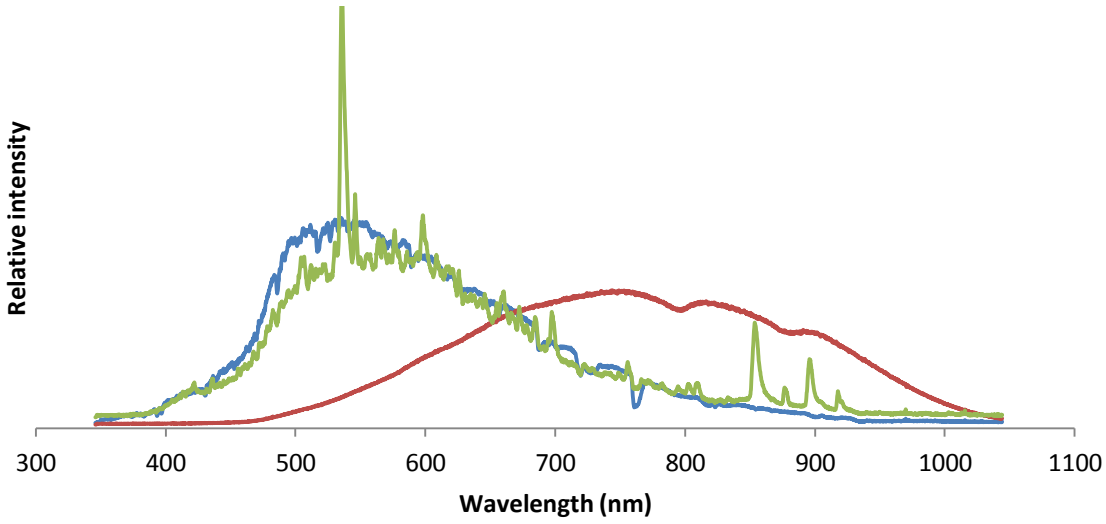

Fig. 11. Spectra of incident light during cell growth. Earth surface radiation (blue), high/low light conditions (green), red light conditions (red). Measured with Ocean Optics USB4000 spectrometer. Spectra are normalized to equal areas.

Isolation of thylakoid membranes: The isolation was performed in a dark room with a dim green light, at 0-4 °C (on ice) with cooled apparatus. Thawed sample was washed with buffer (50 mM MES, 6.5 pH, 2mM KCl), centrifuged (1000 g, 5 min), resuspended in the same buffer and protease inhibitor (cOmplete EDTA-free, Roche Diagnostics) was added. Further, cells were disrupted at 16 000 PSI using EmulsiFlex-C5 (Avestin Inc., Canada) and centrifuged (1000 g, 5 min). Supernatant was collected and centrifuged (60 000 g, 40 min). The pelet from the last centrifugation was resuspended in buffer (50 mM MES, 6.5 pH, 2mM KCl). Chlorophyll concentration was determined according to Lichtenthaler (Lichtenthaler 1987).

Thylakoid solubilization and sucrose gradient: Thylakoid membranes, corresponding to 250 μg of chlorophyll in 500 μL solution, were solubilized with detergent (tab. I) for 30 min while stirring on ice. The sample was centrifuged (30 000 g, 30 min) and supernatant (400 μL) was loaded on a 0-1 M continuous sucrose gradient, prepared by freeze-thaw method, containing 50 mM MES (6.5 pH), 0.55 M sucrose, 2 mM KCl and 0.02 % corresponding detergent (tab I.), followed by ultracentrifugation (150 000 g, 16 h, 4 °C) using a SW-40 swing-out rotor (Beckman Coulter).

Table I

Detergents and concentrations used for thylakoid solubilization.

	Mw (g/mol)	Concentrations used (m/V)
n-Dodecyl β-D-maltoside	510.62	0.5 %, 1 %, 2 %, 4 %
n-Dodecyl α-D-maltoside	510.62	1 %, 2.5 % 3 %
Digitonin	1229.31	1 %, 2.5 % 5 %

Gradient zone collection, fluorescence measurement and sample concentration: Visible zones were collected using syringe. Fluorescence emission 77K (620-780 nm) was measured using a Spex Fluorolog-2 spectrofluorometer (Jobin Yvon, Edison, NJ, USA) (excitation wavelength: 435 nm). Further, each zone was concentrated and washed with isolation buffer (50 mM MES, 6.5 pH, 2 mM KCl) containing 0.02 % detergent to get rid of excess sucrose, using Amicon Centrifugal filters 30k (10 000 g). Concentrated samples were kept on ice in dark and analyzed by further methods.

SDS-PAGE, ion exchange chromatography, UV-VIS absorption: SDS-PAGE from selected gradient zones was performed on a 14 % isocratic acrylamide gel SERVAGel^{TM} in denaturing conditions according to Laemmli (1970). 25 mM Tris, 192 mM glycine and 1 % SDS was used as running buffer. The gels were stained by coomassie blue and/or using silver staining. Anionic exchange chromatography was performed using DEAE Sepharose CL-6B as stationary phase at the pH of 6.5. Isolation buffer with 0.02 % detergent and linearly increasing concentration of NaCl (0.005 – 0.5 mol/L) was used as mobile/elution phase at a flow of 1 mL/min. Absorbance was measured using SHIMADZU UV-2600 absorption spectrophotometer.

Clean native electrophoresis and 2D SDS-PAGE: The elucidation of protein-complex content of the sucrose gradient zones, from cells grown on red light, was done using clean native electrophoresis, according to Komenda e*t al.* (2012), on 4-14 % linear gradient acrylamide gel, followed by second SDS-PAGE dimension using 12-20 % linear gradient gel containing 7 M urea. Acrylamide/bisacrylamide ratio in both gels was 38. The gel was stained using coomassie blue.

Thylakoid isolation from *Pisum sativum*:. The plant was grown in a greenhouse. Leaves were harvested in early summer (June), homogenized in 50 mM tricine, 0,4 M sorbitol, 5 mM $MgCl_2$, 10 mM KCl, 1 mM $MnCl_2$ and 1 % (m/V) BSA. The mixture was centrifuged (1500 g, 2 min), supernatant was again centrifuged at 5000 g (10 min). The pellet was resuspended and used for detergent solubilization with same conditions as noted above for *T. minutus*.

Fluorescence spectra normalization and fitting method

Fluorescence spectra were normalized to equal heights. Fitting in figure 33 was done in following way. Each fraction spectrum was multiplied by a constant. The constants were varied until the area of their sum was the closest to the area of the zone spectrum.

2.1 Principles of used methods

Separation methods

Non-equilibrium ultracentrifugation on a sucrose gradient

Non-equilibrium centrifugation on a gradient is used to separate analytes according to their size. All molecules/complexes loaded on top of the gradient are forced by the centrifugal force to move along the gradient, with larger complexes moving faster, because they experience larger g force, given that all separated complexes have similar density. The centrifugation has to be stopped before the complex of interest reaches the bottom of the gradient, which would prevent its separation.

SDS-PAGE / clean native electrophoresis

Electrophoresis on a gel is used for protein separation. They are separated by difference in their movement speed through the gel. The speed is determined by the size/surface charge ratio of the polypeptide/complex. Larger and less charged complexes move slower. All separated complexes need to have same overall charge polarity (introduced by use of detergent) to move in the same direction. The native electrophoresis is used for protein separation in their native state. Either colored or colorless detergent is used, determined by the need for later spectroscopic analysis of the separated complexes. In SDS-PAGE a sodium dodecyl sulfate (SDS) is used for charge introduction along with a reducing agent and heat for denaturation, resulting in division of fully denatured polypeptides.

Ion exchange chromatography

Ion exchange is used to separate molecules/complexes according to their surface charge properties. A column which contains counterions to our molecules of interest, at a given pH or salinity, has to be used. Analytes bind to the stationary phase and are eluted by a gradient of either salt or pH. Weakly surface charged molecules elute first.

Spectroscopic methods

Fluorescence emission

Fluorescence is a deexcitation of a molecules valence electron by a photon release. It can be used to get information about the electronic properties of a molecule. An excited electron usually loses some energy due to thermal exchange, moving itself to a more stable (less energetic) excited state, resulting in the red shift of emission spectra compared to absorption. Each chromophore has characteristic maximum of emission wavelength, which corresponds to the energy difference between the most probable excited state and the ground state. At 77 Kelvin, less energetic states get much more probable, resulting in a shift of maximum towards longer wavelength and narrowing of the spectrum.

UV/VIS absorption

Absorption spectroscopy, in the ultraviolet and visible regions, is used to get information about the electronic properties of a chromophore in range of 200-800 nm. Nonbonding and π electrons absorb in this region. Dependence of absorbance on the incident photon wavelength is measured. Each chromophore absorbs energy equal to the difference between HOMOs and the accessible LUMOs. The probability of absorption and the corresponding peak size is determined by the size of the dipole created on the molecule by electron excitation.

3. Results

The reason for our interest in light harvesting complexes of *Trachydiscus minutus* was the measured difference in absorption and fluorescence of cells cultivated under high light and red light conditions as shown in figures 12 and 13.

The absorbance of cells grown under red light (fig. 12, red line) is compared first, it shows around 50% increase between 700 and 710 nm compared to blue light variant (fig.12, blue line), yet almost exact match in higher energies below 679 nm. Secondly the fluorescence spectrum of red light grown cells (fig. 13, red line) is shifted towards lower energy for ~9 nm and has decreased intensity in the left side of the peak compared to blue light variant (fig. 13, blue line).

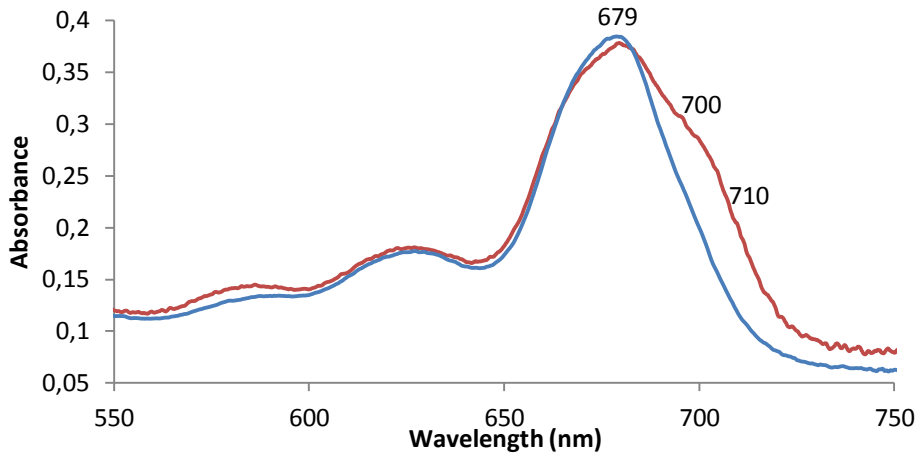

Fig. 12. Comparison of absorption spectra of *T. minutus* grown under high light (blue line) and red light (red line) conditions.

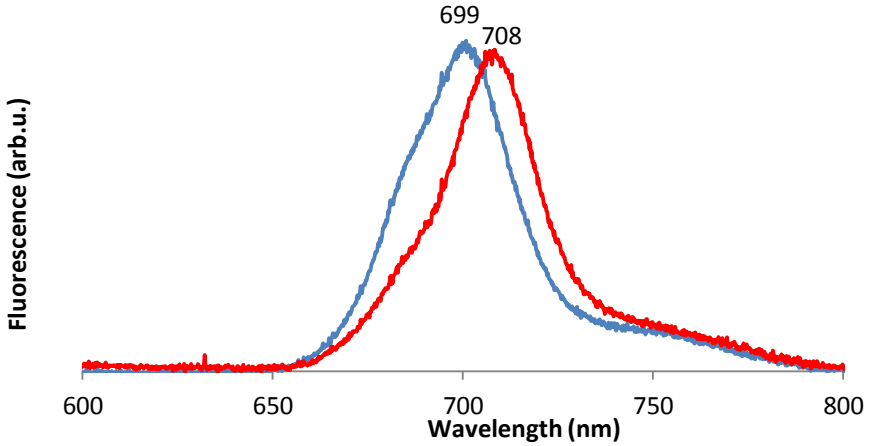

Fig. 13. Comparison of 298 K fluorescence spectra of *T. minutus* cells grown under HL (blue) and RL (red) conditions.

Aim of this work was first to find a suitable detergent and its concentration which would allow separation of light absorbing complexes from *T. minutus* using sucrose gradient. This method was then used to help explain the different behavior shown on figures 12 and 13. The sucrose gradient along with spectroscopic methods for characterization of native pigment protein complexes from Eustigmatophyceae were used previously (Arsalane *et al.* 1992, Basso *et al.* 2014).

3.1 Sucrose gradient optimization

Before the investigation of the chromatic adaptation, suitable conditions for thylakoid isolation and solubilization were explored. The detergent effectivity was tested on HL grown samples, because they usually contain the biggest amount of fatty acids (which interfere with the thylakoid purification). Three detergents (n-dodecyl β-D-maltoside, n-dodecyl α-D-maltoside, digitonin) at various concentrations (tab. I) were used to solubilize isolated thylakoids from *T. minutus*. Sucrose gradient of the solubilized thylakoids, SDS-PAGE and fluorescence 77K of the gradient zones were used to get a basic insight in the effectivity of complex solubilization and separation. The overview of these gradients is depicted in figures 14 and 15. The sucrose gradient method for light harvesting protein complex separation was employed on solubilized thylakoids of pea (fig. 14) to get a visual comparison with higher plant.

Further analysis of the collected zones as depicted in figures 14 and 15 was done by SDS-PAGE and fluorescence. Interpretation of these results (which are described in the following three sections 3.1.1, 3.1.2 and 3.1.3), was based on the data reported in section 3.2.1 (figures 29, 30 and 31).

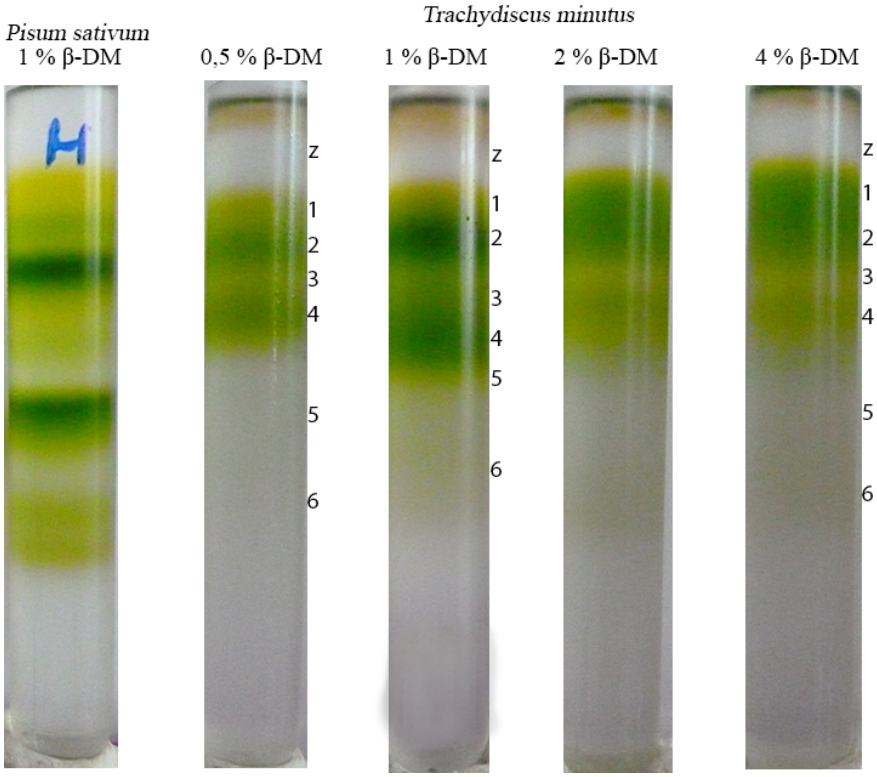

Fig. 14. Comparison of sucrose gradients of solubilized thylakoids of *T. minutus* and *P. sativum* by n-dodecyl β-D-maltoside, zones for SDS-PAGE and fluorescence measurement were collected as displayed.

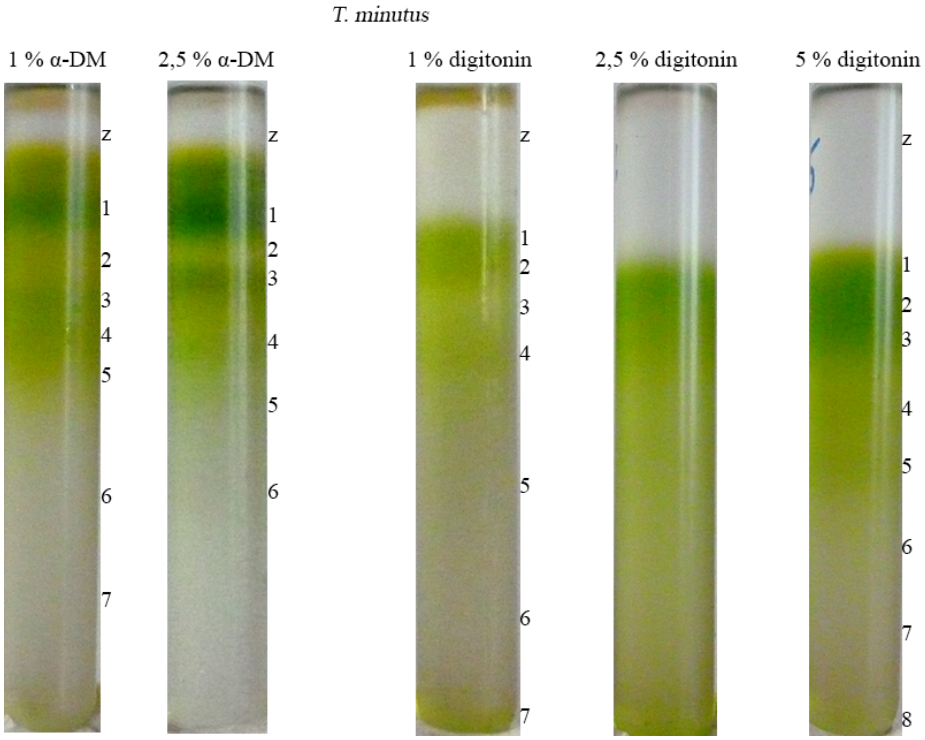

Fig. 15. Comparison of sucrose gradients of solubilized thylakoids by n-dodecyl α-D-maltoside and digitonin, zones for SDS-PAGE and fluorescence measurement were collected as displayed.

3.1.1 n-dodecyl β-D-maltoside

First investigated detergent for solubilization of light absorbing complexes from thylakoid membranes was β-D-maltoside at concentrations 0.5, 1, 2, and 4%. Solubilized complexes were then separated on sucrose gradients as shown in figure 14. The composition of collected zones was further investigated using 14% isocratic SDS-PAGE and fluorescence at 77K. The analyzed β-D-maltoside gradients are shown along with their respective SDS-PAGE gels in figures 16 and 17.

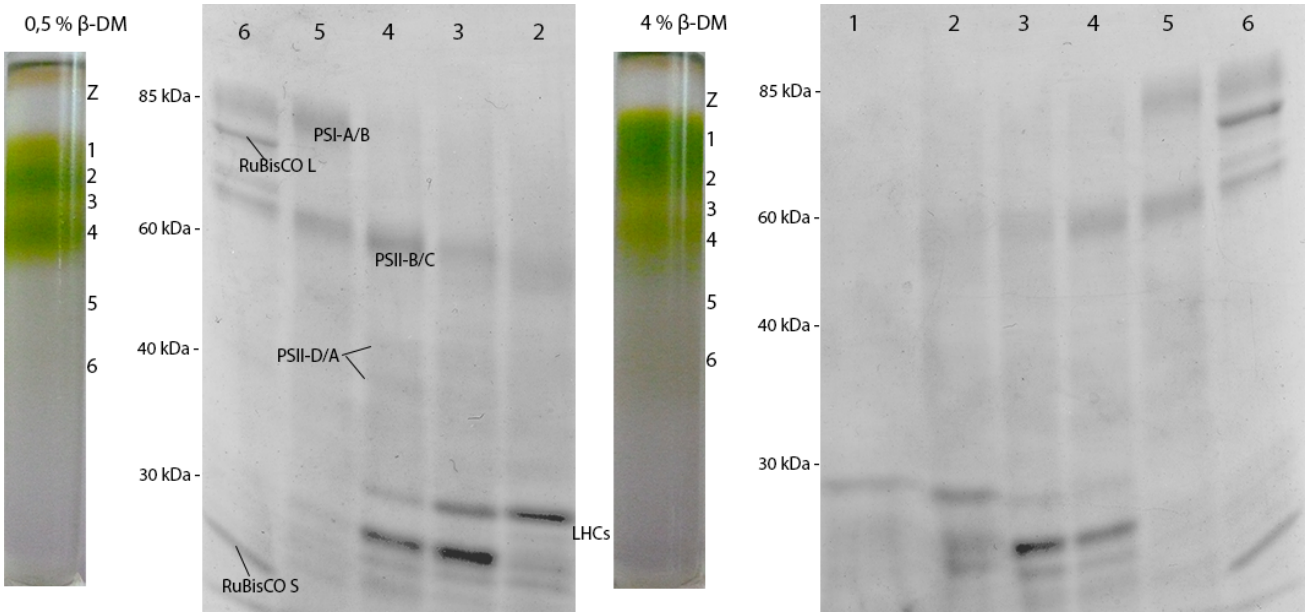

Fig. 16. SDS-PAGE of harvested zones from sucrose gradients made using 0.5 % (right) and 4 % (left) β-D-maltoside. (Note the zones on the two gels are in opposite order.)

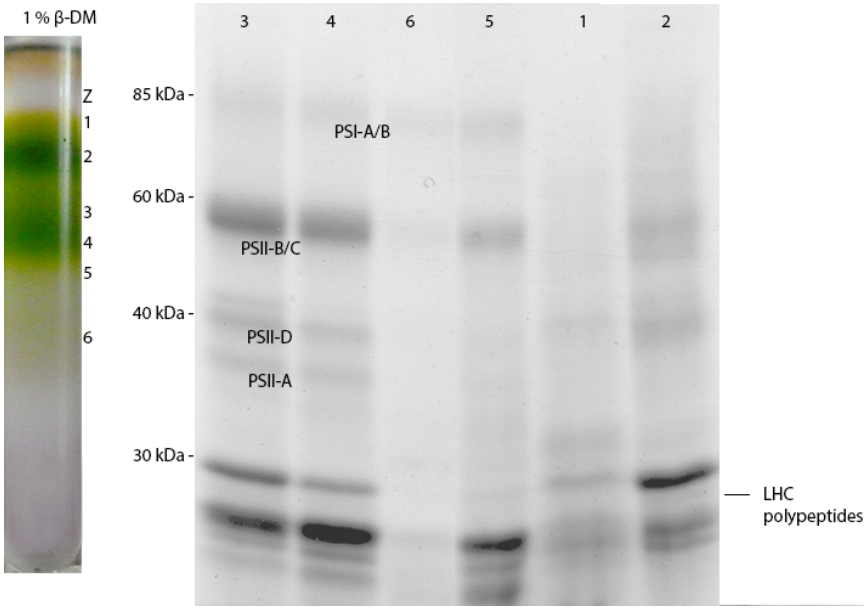

Fig. 17. SDS-PAGE of harvested zones from the sucrose gradient (using 1 % β-DM).

Both photosystem core polypeptides as well as LHC proteins were found using SDS-PAGE in the collected gradient zones as noted in figures 16 and 17. RuBisCO has copurified in last harvested zone as shown in the 0.5 % gradient (fig. 16). Further, the fluorescence emission of marked zones, from 1 % β-DM sample, was measured and compared (figure 18).

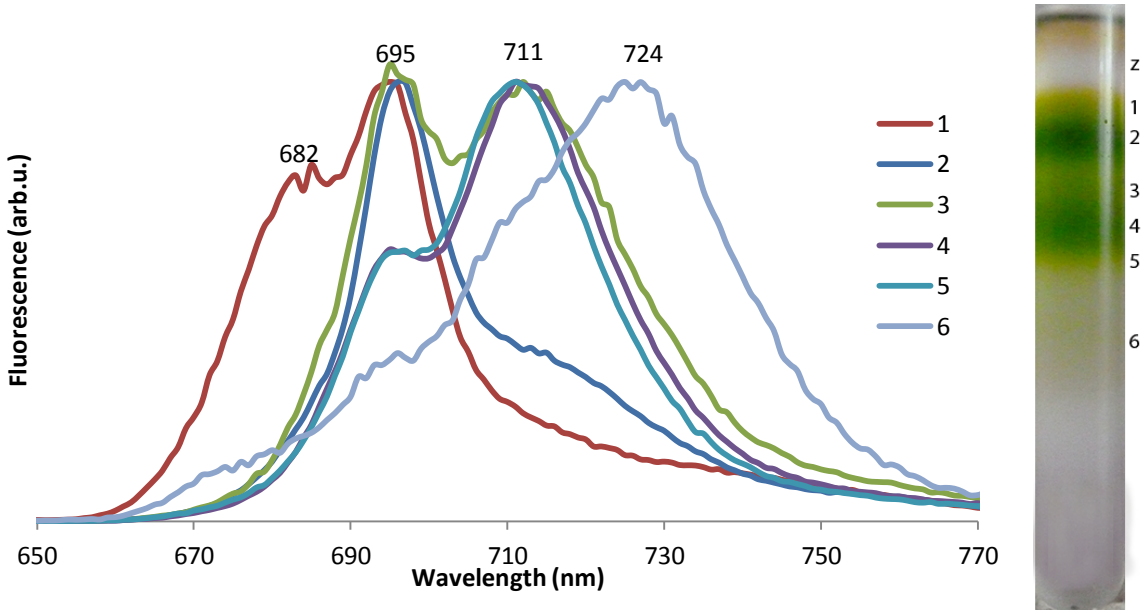

Fig. 18. 77 K fluorescence spectra of marked zones from 1 % β-D-maltoside sucrose gradient.

Four distinct fluorescence maxima were found using β-dodecyl maltoside as detergent (fig. 18). Emission maximum at 724 nm corresponds to PSI as found later (F10 in figure 29), fluorescence with maxima at 711 and 695 nm correspond to LHC oligomers/subunits (F4 and F2 in figure 29). The peaks around 682 nm represent fluorescence of free pigment released from denatured complexes.

To further investigate the effect of different detergent concentrations, fluorescence of the two most chlorophyll dense zones (zone 2 and 4) found in the sucrose gradients are compared for the three selected detergent concentrations (figure 19). All three samples show maxima in the same positions in the second zone. Zone 4 from 1 % β-DM gradient is slightly shifted towards longer wavelength (~2 nm).

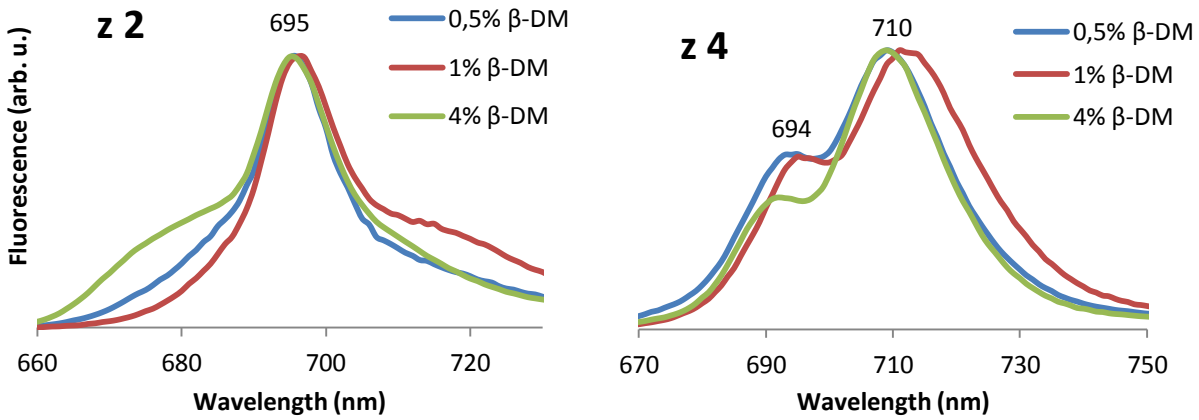

Fig. 19. Comparison of fluorescence spectra of zones 2 (left) and 4 (right) at 77 K from selected β-D-maltoside gradients.

Fluorescence spectra were measured also at room temperature (295 K). Comparisons of zone 2 and 4 fluorescence at 77 K and 295 K from 4 % β-DM gradient are shown in figure 20. Spectra measured at 77 K (dark green and dark purple, fig. 20) have maxima at lower energy (shifted by around 9 nm) compared to room temperature fluorescence (light green and light purple, fig. 20). Also note that the spectra are narrower at lower temperature.

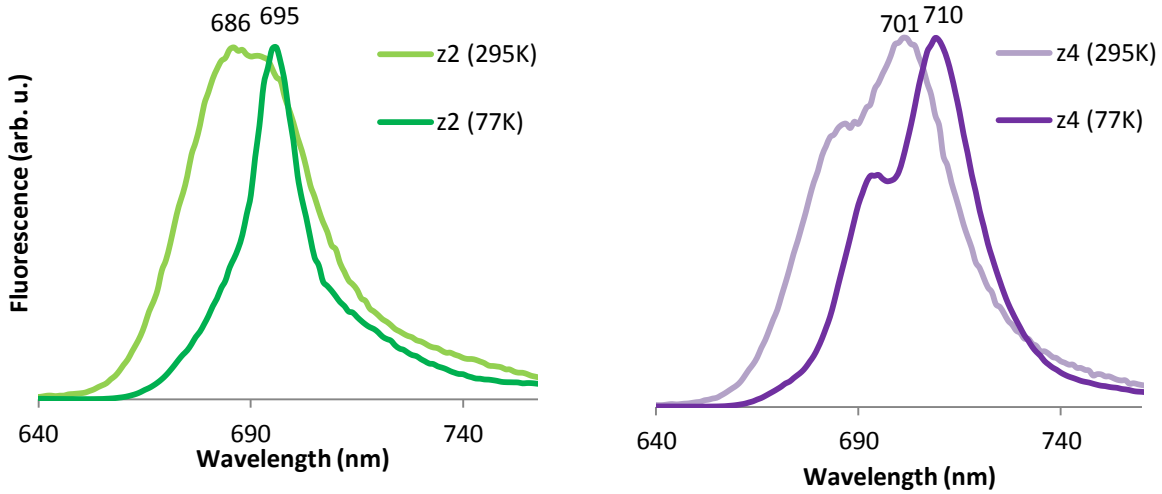

Fig. 20. Comparison of room temperature (295 K) and 77 K fluorescence spectra of zones 2 (left) and 4 (right) from 4 % β-DM sucrose gradient.

3.1.2 Digitonin

Digitonin was selected as the next detergent for the light absorbing complexes investigation. Concentrations of 1, 2.5 and 5 % were employed for thylakoid solubilization. Resulting gradients are depicted in figure 15. Further, 1 and 5 % digitonin gradients were selected for SDS-PAGE (fig. 21) and fluorescence (figures 22 and 23) measurements. All the expected light harvesting complexes (PSI core, PSII core and LHC proteins) were found in the 5 % digitonin gradient. The acrylamide gel from 1 % digitonin gradient showed insufficient complex solubilization. Only LHCs and traces of PSII were observed.

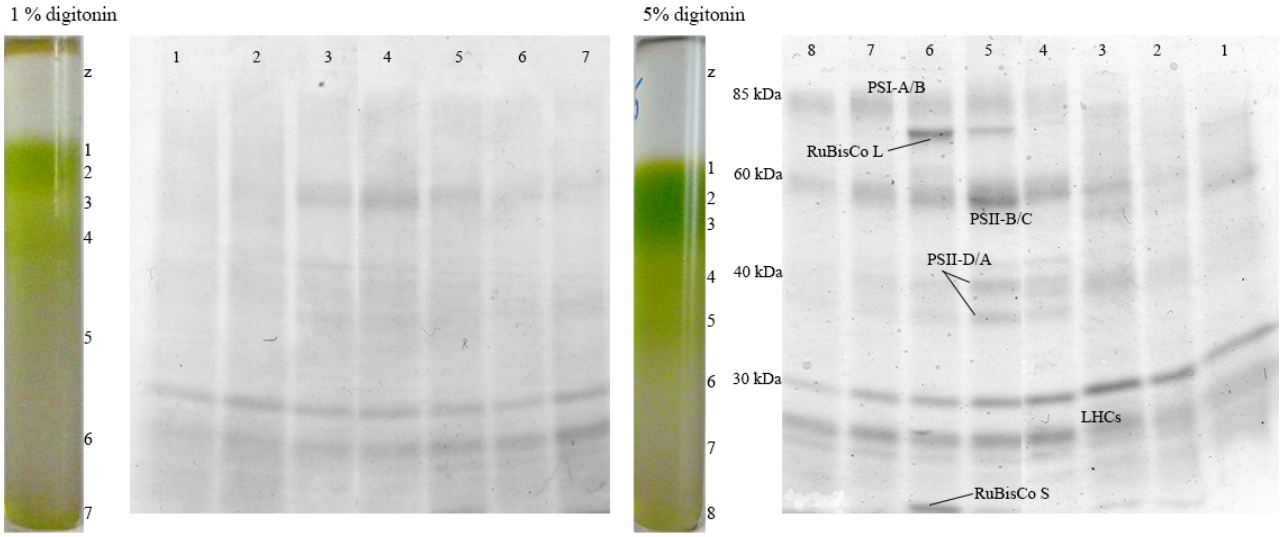

Fig. 21. SDS-PAGE of harvested zones from gradients made using 1 and 5 % digitonin as thylakoid solubilization agent. (Note the zones on the two gels are in opposite order.)

Further, the fluorescence spectra from 1 and 5 % digitonin gradients are shown in figures 22 and 23. Three distinct maxima were found when analyzing the 1 % digitonin gradient by 77 K fluorescence. The fluorescence maximum at 684 nm corresponds to free pigments, 695 and 711-712 nm maxima are LHC subunits and oligomers (F2 and F4, figure 29). In the 5 % digitonin gradient the PSI fluorescence (720-725 nm) becomes visible in the bottom zone of the gradient (fig. 23, line 8).

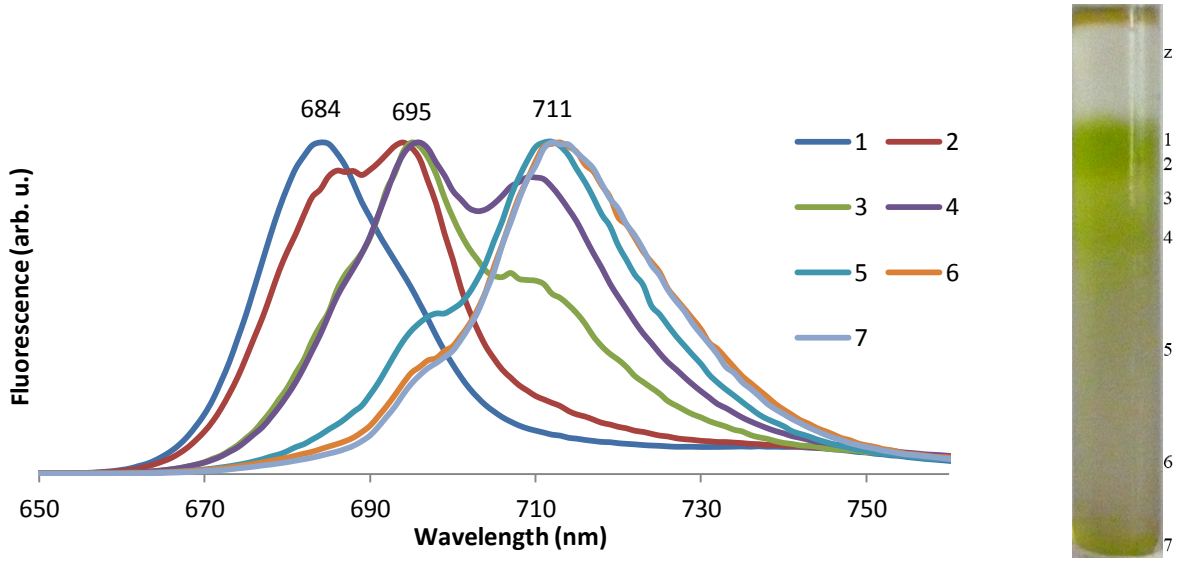

Fig. 22. Fluorescence spectra at 77 K of sucrose gradient zones (1 % digitonin).

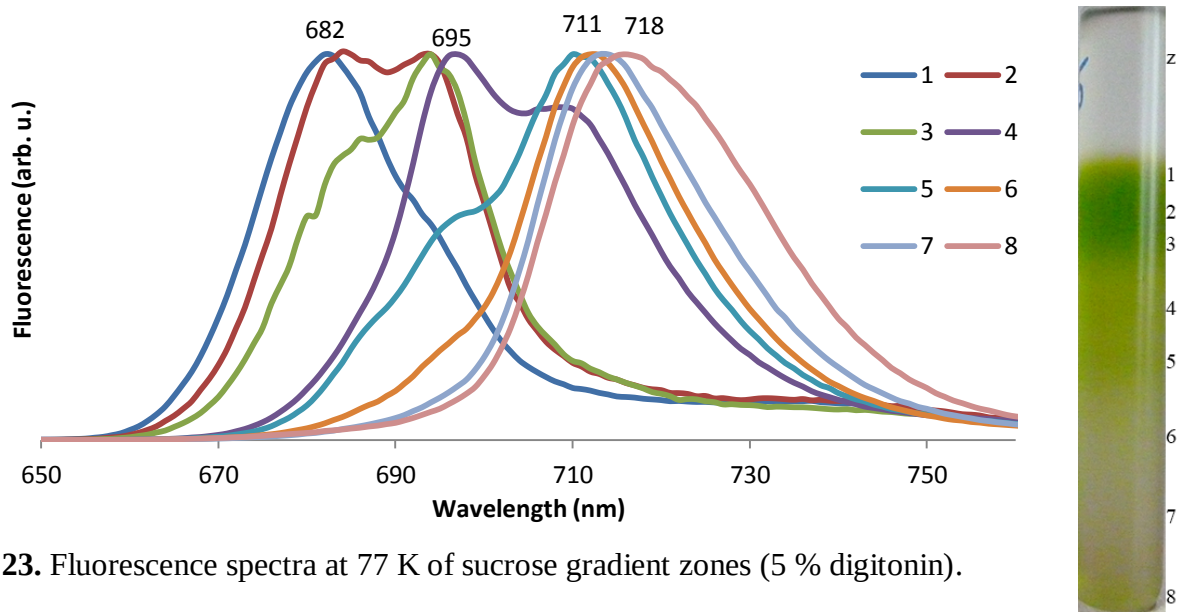

Fig. 23. Fluorescence spectra at 77 K of sucrose gradient zones (5 % digitonin).

3.1.3 n-dodecyl α-D-maltoside

The third and last detergent tried for the optimization of thylakoid solubilization was n-dodecyl α-D-maltoside at 1 and 2.5 % concentration. SDS-PAGE of gradient zones is shown on figure 24. The same polypeptides were found using the electrophoresis on α-D-maltoside gradient zones as in the previous cases, but in the 2.5 % α-D-maltoside concentration the complexes are much more localized to certain height in the sucrose gradient as is apparent from the SDS-PAGE (fig. 24).

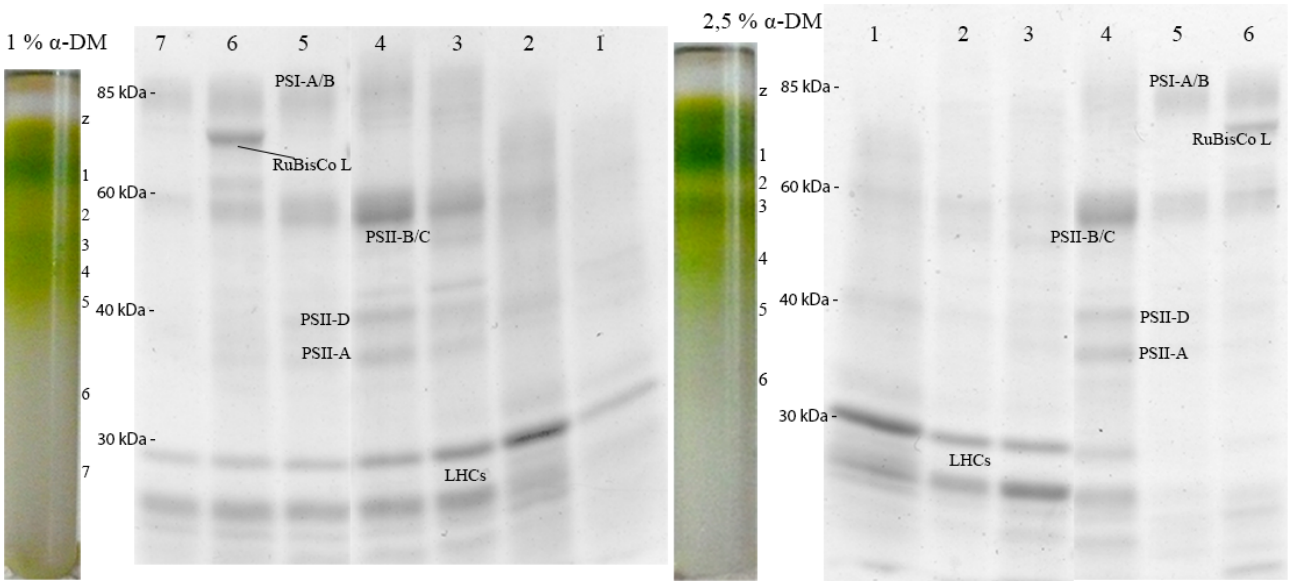

Fig. 24. Sucrose gradients and SDS-PAGE of the harvested zones, as marked. α-D-maltoside at 1 % concentration (left) and 2.5 % concentration (right) was used for thylakoid solubilization. (Note the zones on the two gels are in opposite order.)

Same as in previous cases the fluorescence of the gradient zones was measured and is shown in figures 25 (1 %) and 26 (2.5 %). There were four fluorescence maxima identified in the 1 % α-DM gradient (fig. 25). Fluorescence maximum at 680 nm belongs to free pigment. The maxima at 695 and 711 nm belong to LHC oligomers/subunits (F2 and F4 in figure 29), exactly same as in previous cases. The maximum at 722-724 belongs to PSI (F10 in figure 29).

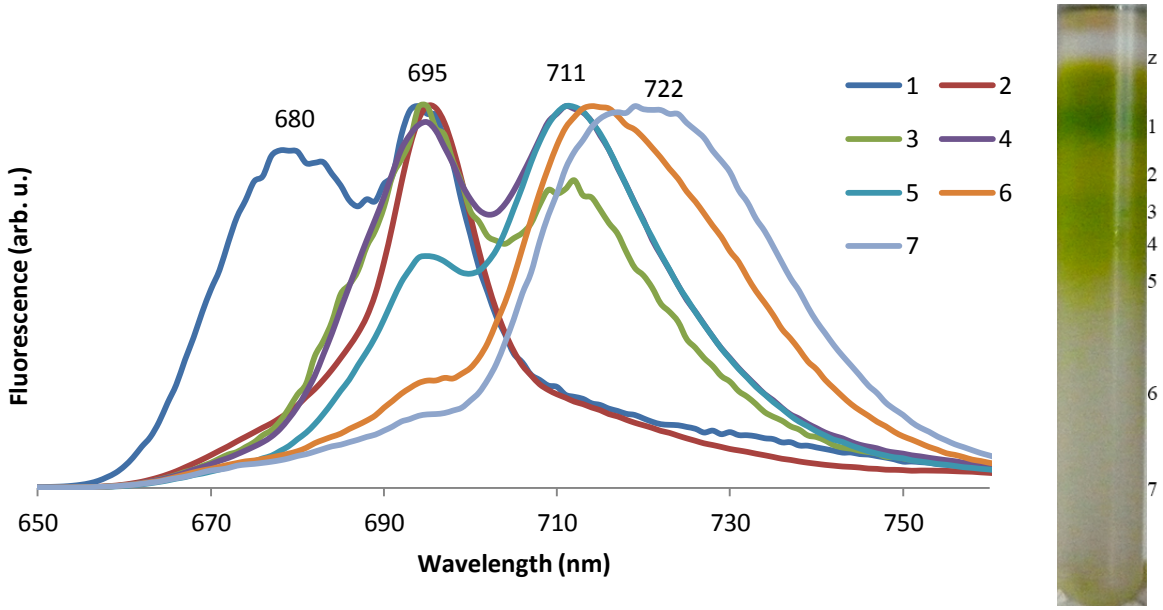

Fig. 25. Fluorescence spectra at 77 K of sucrose gradient zones (1 % α-D-maltoside).

In the 2.5 % α-D-maltoside gradient (fig. 26) a new fluorescence maximum was found, in the zones 4 and 5 (at 690 nm, belonging to PSII, F5 and F7 in figure 29), which was not found in previous cases. The other three maxima (695, 711 and 725 nm) correspond with results from 1 % α-DM (fig. 25).

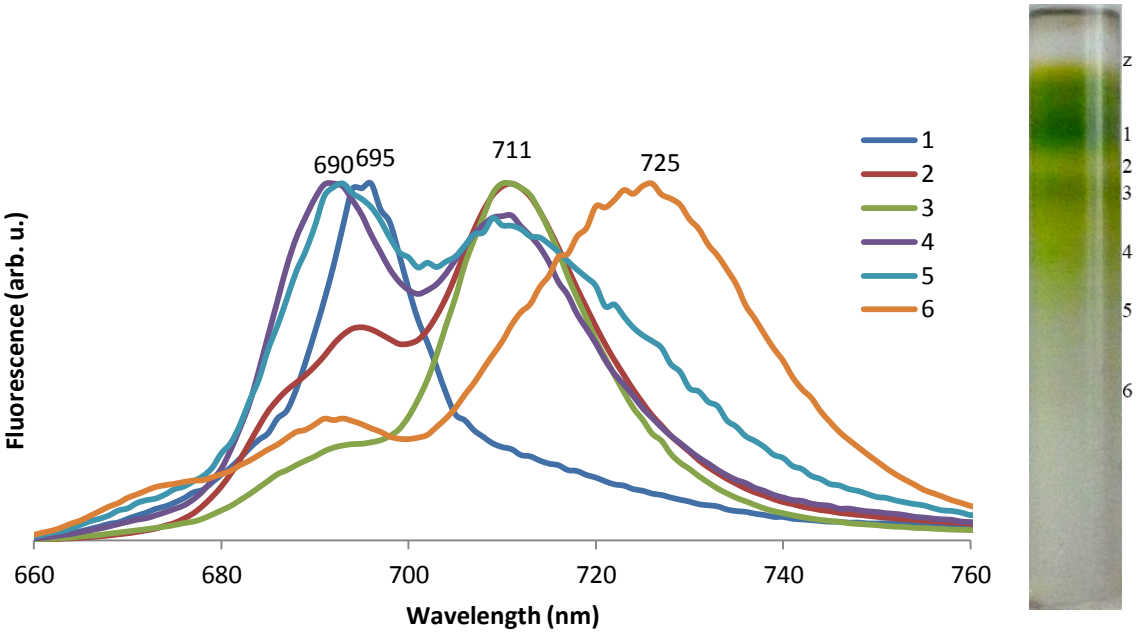

Fig. 26. Fluorescence spectra at 77 K of sucrose gradient zones (2.5 % α-D-maltoside).

For further investigation of the chromatic adaptation α-D-maltoside was chosen at 3 % concentration, based on the results from 2.5 % gradient (fig. 26). α-D-maltoside provided better focus of the isolated complexes into narrow gradient zones compared to other detergents/concentrations, also PSII was localized almost exclusively into one zone, having maximum fluorescence at 690 nm, which was not found previously. Also no LHC proteins were found in the bottom half of the gradient in the 2.5 % α-DM.

3.2 Investigation of the chromatic adaptation in *T. minutus*

After obtaining substantial amount of data about HL grown samples during the detergent optimization, isolated thylakoid membranes from RL and LL samples were solubilized by 3 % n-dodecyl α-D-maltoside and separated on sucrose gradients. They are depicted in figure 27 along with the lower part of their SDS-PAGE (14 % isocratic gel) of zones 2, 3a, 3b and 4 from each gradient (figure 27).

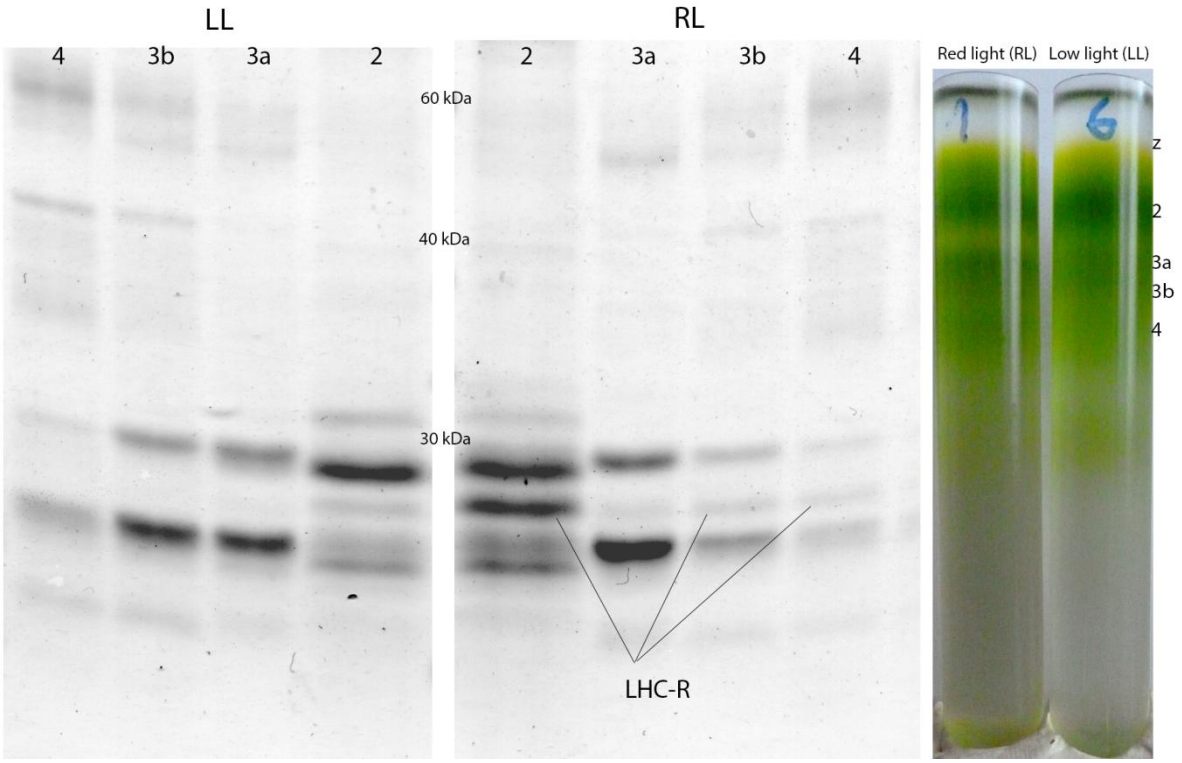

Fig. 27. SDS-PAGE comparison of antennae sized polypeptides from cells grown under the same light intensity (15 μmol photons.m^{-2}.s^{-1}) with different spectra (fig. 1). The increased presence of polypeptide LHC-R in the RL variant is depicted. (Note the zones on the two gels are in opposite order.)

Increased presence of one LHC-sized polypeptide was found inside the gradient of RL variant (compared to HL and LL variants). This polypeptide was named as LHC-R. It is important to consider at this point that zone 3b and zone 4 (figure 27) were the only zones which showed different fluorescence when comparing the RL and LL sample. Therefore further investigation was focused on them. The comparison of fluorescence spectra of zones 3b and 4 from RL and LL is shown in figure 28. No differences in fluorescence maxima were measured in zones 2 (694 nm maximum) and 3a (710 nm maximum) and anywhere below the zone 4 of the two

gradients. On the other hand zone 4 had two maxima from which one (691 nm) is exactly in the same position in LL as in RL, and the second one is strongly shifted to lower energy in the RL sample.

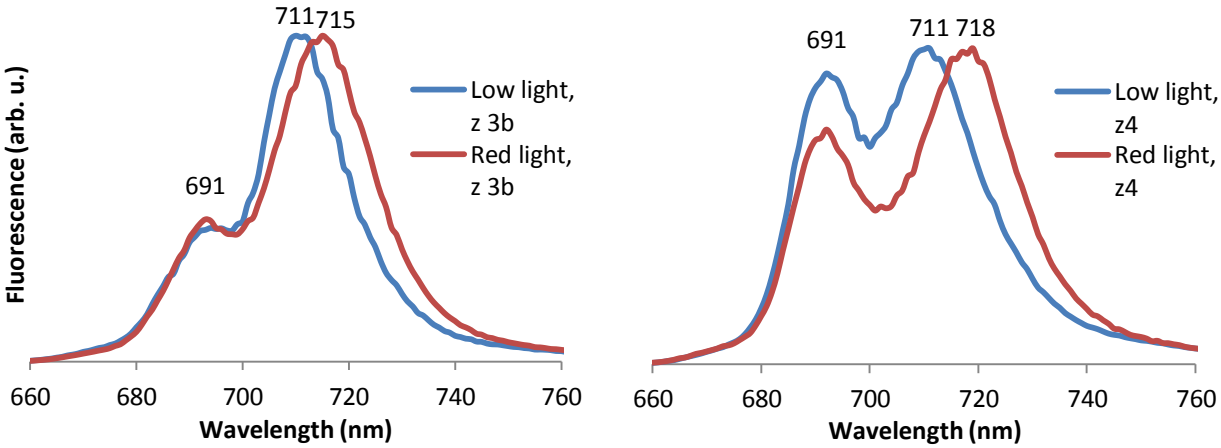

Fig. 28. Comparison of 77 K fluorescence of the zones 3b (left) and 4 (right) from sucrose gradients made using LL and RL cells from figure 27. Zone 4 from all three variants HL, LL and RL is compared in figure 32.

Two separation methods were further used to get more information about the fluorescence difference found between zones 3b and 4 in RL and LL samples and about the role of LHC-R in it. One was clean native electrophoresis of the gradient zones followed by 2D SDS-PAGE (section 3.2.1). The second one was ion exchange chromatography of zones 3 and 4 (section 3.2.1).

3.2.1 Clean native electrophoresis

To elucidate the origin of a fluorescence maximum at ~718 nm present around the middle of the RL sucrose gradient (zone 4 RL, figures 27, 28), which was not found in HL and LL samples, clean native electrophoresis of the RL gradient zones and solubilized thylakoid membranes was performed (fig. 29). The detergent used for RL grown *T. minutus* thylakoid solubilization was n-dodecyl α-D-maltoside at 3% (m/V) concentration. 0-1 M continuous sucrose gradient was employed for the separation, followed by fluorescence measurement (77K) of complexes found in the clean native gel (fig. 30).

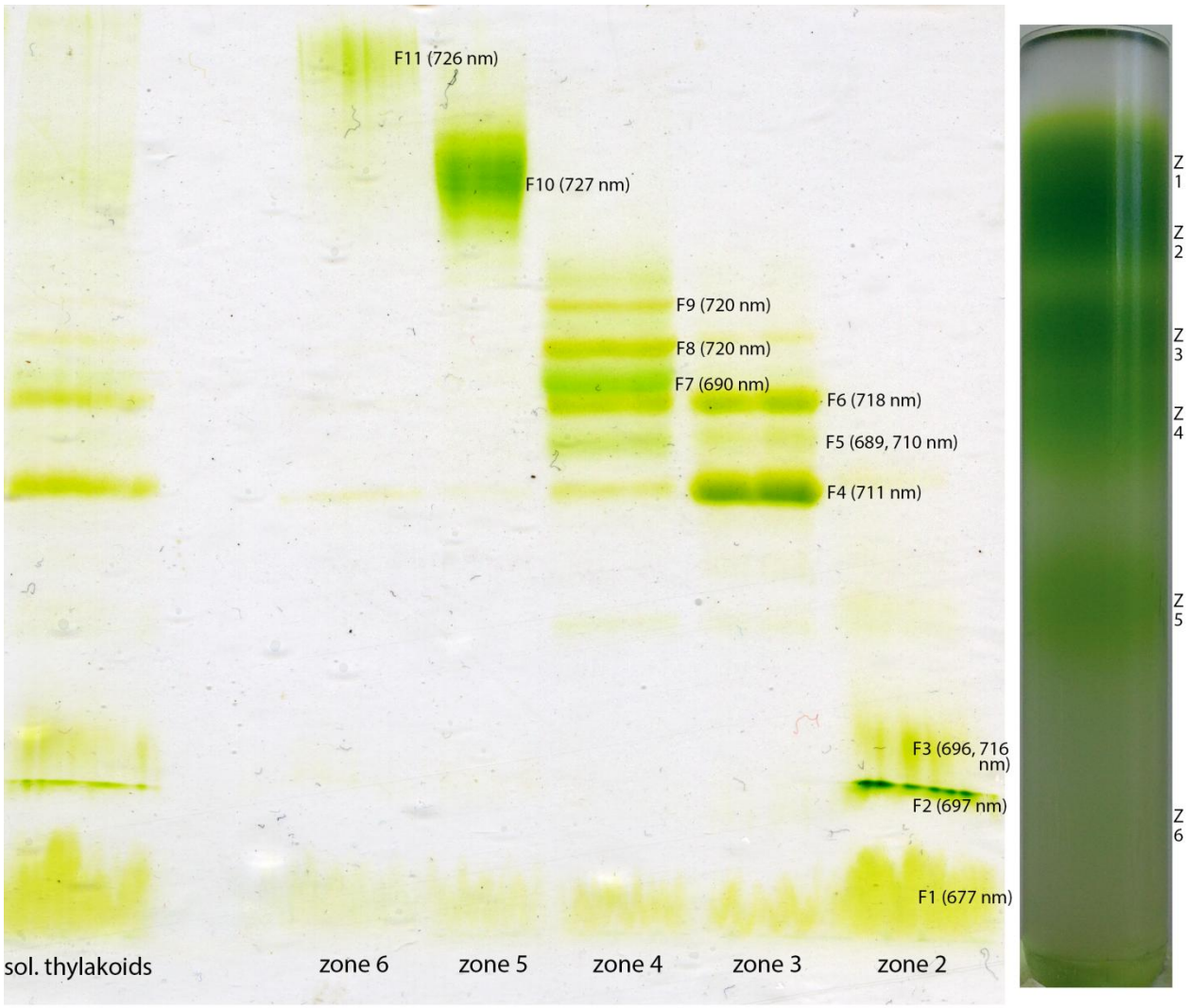

Fig. 29. Clean native electrophoresis of harvested zones from the sucrose gradient and solubilized thylakoids (both RL grown, 3% α-D-maltoside). 5 μg of chlorophyll was used for each line. Labels F1-F11 designate fractions further studied by fluorescence emission and/or 2D SDS-PAGE. Numbers in the parentheses denote a fluorescence maximum of the fraction at 77K. Fractions F3 and F5 had two maxima. Zone 1 was omitted from the electrophoresis due to almost exclusive presence of free pigment.

At least 10 distinct complexes were found in the resulting CN gel, with the widest variety found in zones 3 and 4, where the fluorescence difference between HL, LL and RL variants was found previously. To identify the nature of these complexes, second dimension SDS-PAGE on 12-20% linear gradient acrylamide gel was done (fig. 31), along with fluorescence measurement of each complex (fig. 30). Lines of CN gel served as the first dimension for 2D-SDS-PAGE.

Using the information from 2D SDS-PAGE (figure 31), PSI and PSII cores were identified in zones z5 and z4 as fractions F10 and F7 respectively. Fraction F5 was judged to be PSII core lacking subunit PSII-C. All other fractions (F2, F3, F4, F6, F8 and F9) in figure 29 were judged to be antenna complexes, based on their protein sizes.

Fluorescence of each complex marked in the CN was measured at 77K (figure 30). Following the results from 2D SDS-PAGE, each complex was assigned its characteristic 77K fluorescence maximum. Using the data from this section, the fluorescence spectra and SDS-PAGE gels from section 3.1 were retrospectively identified.

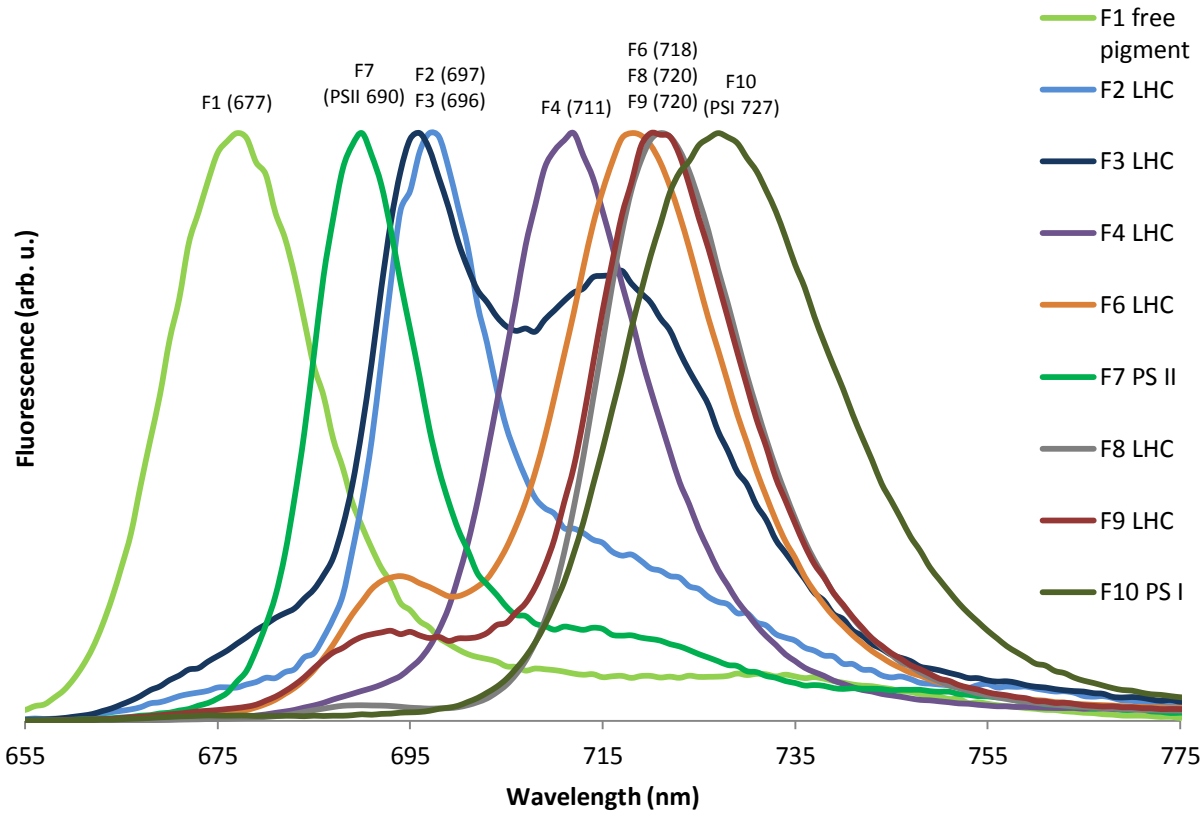

Fig. 30. Fluorescence spectra at 77K of complexes from native electrophoresis (fig. 29), fractions F5 and F11 were omitted from this figure for better clarity. Three maxima belonging to LHC antenna complexes were identified 696, 711 and 720 nm. PSI emits at 727 nm, PSII at 690 nm and free pigment at 677 nm.

The CN in figure 29 was used for 2D SDS-PAGE analysis as shown in figure 31. By analogy with other reports of Heterokont algae, (Grouneva *et al.* 2011, thylakoid membrane complexes analysis of two diatoms by 2D SDS-PAGE), the photosystems were identified.

Green-yellow complexes which were composed of proteins with sized from 20-30 kDa (F2, F3, F4, F6, F8 and F9) were all judged to be various antenna oligomeric stages or antenna monomers.

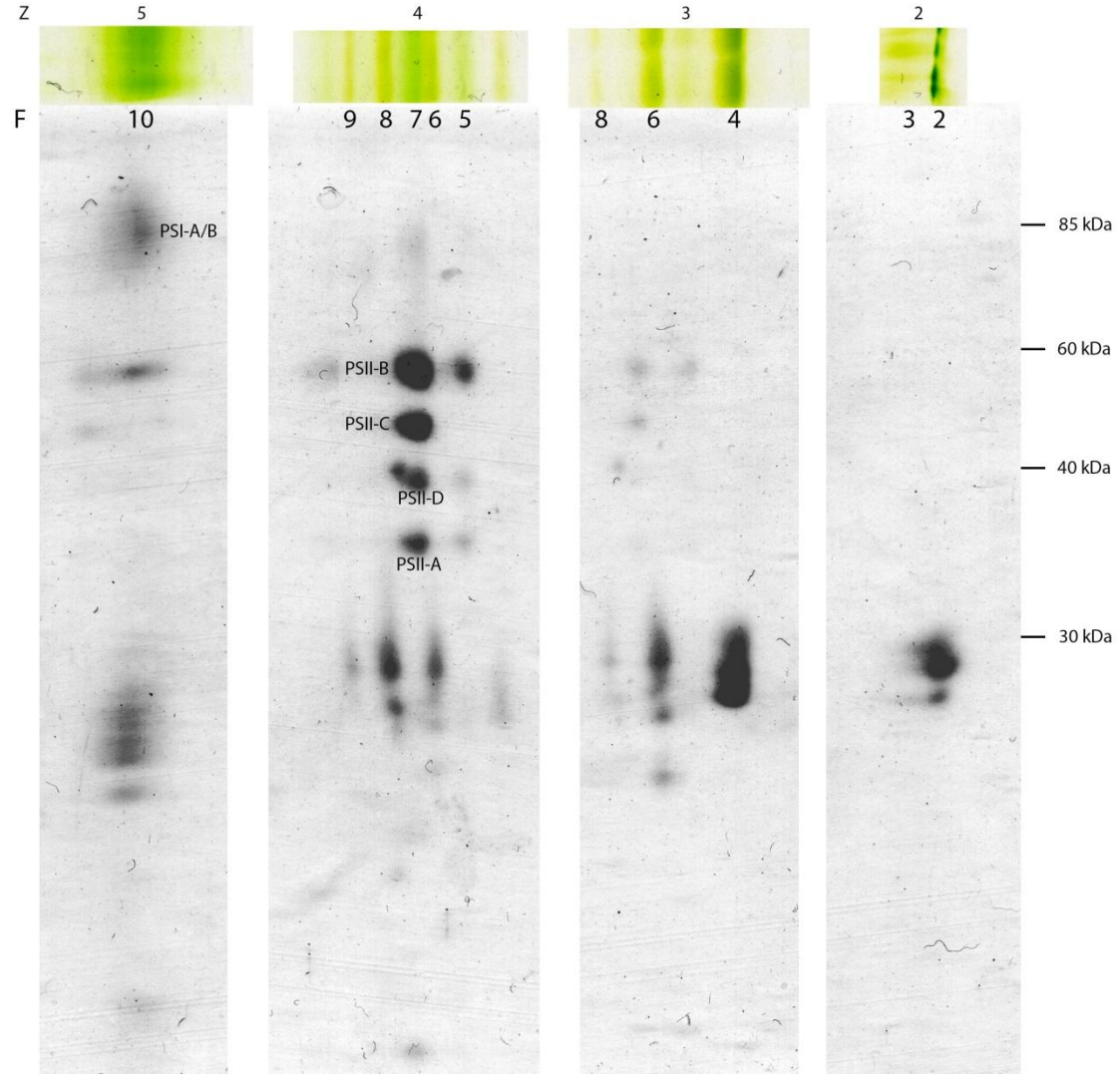

Fig. 31. Two-dimensional SDS-PAGE (12-20% acrylamide) resolution of the light harvesting complexes from *T. minutus*. Lanes of native gel (see fig. 29) were cut out and transferred horizontally on a SDS gel as shown. It was possible to distinguish based on polypeptide sizes which complex is PSI (F10), PSII (F7 and F5) and antenna systems (F2, F3, F4, F6, F8, F9).

Further, the fluorescence emission difference between HL, LL and RL variants found in previous sections was analyzed using gathered fluorescence data.

3.2.2 Analysis of the chromatic adaptation using fluorescence data

To determine how much the red antenna complexes (F6, F8 and F9, fig. 29) contribute towards the detected difference in figure 28, fluorescence spectra of zone z4 from HL, LL and RL version (fig. 32) were fitted with fluorescence spectra of complexes found and measured in the CN (figure 29), the fitting is shown in figure 33 for each variant. For the purpose of this fitting, the red oligomers F6, F8 and F9 (from figure 30) were all represented by the spectrum of F8 (because of their similar fluorescence), and they were called "red antenna". The F4 antenna (figure 30) is here called "blue antenna". Fraction F7 is called PSII core and fraction F5 is called partial PSII core, for reasons mentioned in previous section.

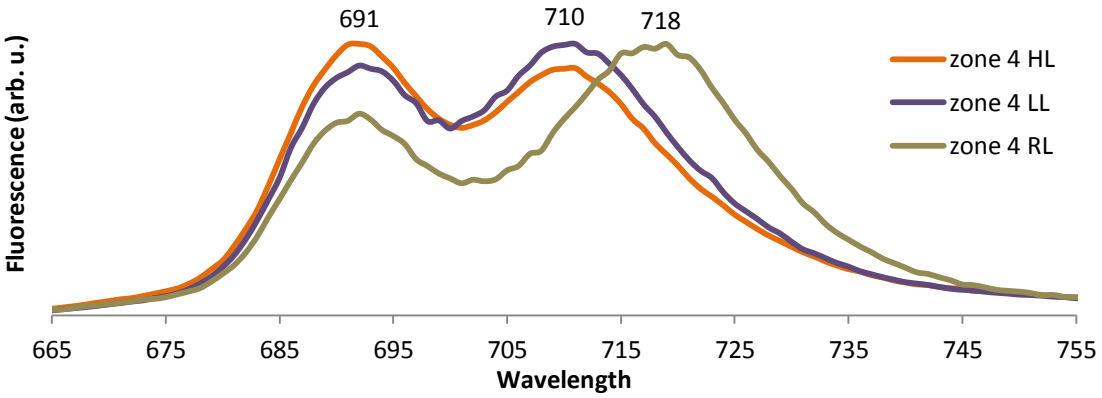

Fig. 32. Comparison of 77 K fluorescence spectra of zones 4 using HL, LL and RL cell variant. Spectra are the same as in figure 26 (zone 4, purple) and in figure 28.

When comparing the HL, LL and RL variants (figure 33, HL-top, LL-middle, RL-bottom), two trends were noticed. Firstly the fluorescence contribution of PSII compared to antennas is the highest in the HL and lowest in the RL variant. On the other hand the presence of antennas shows opposite trend. Further, there is more contribution of blue antenna in the LL version compared to HL version. Also, the right part of the RL zone spectrum consists mainly of the red antenna, which contribution was not present in HL and LL variants.

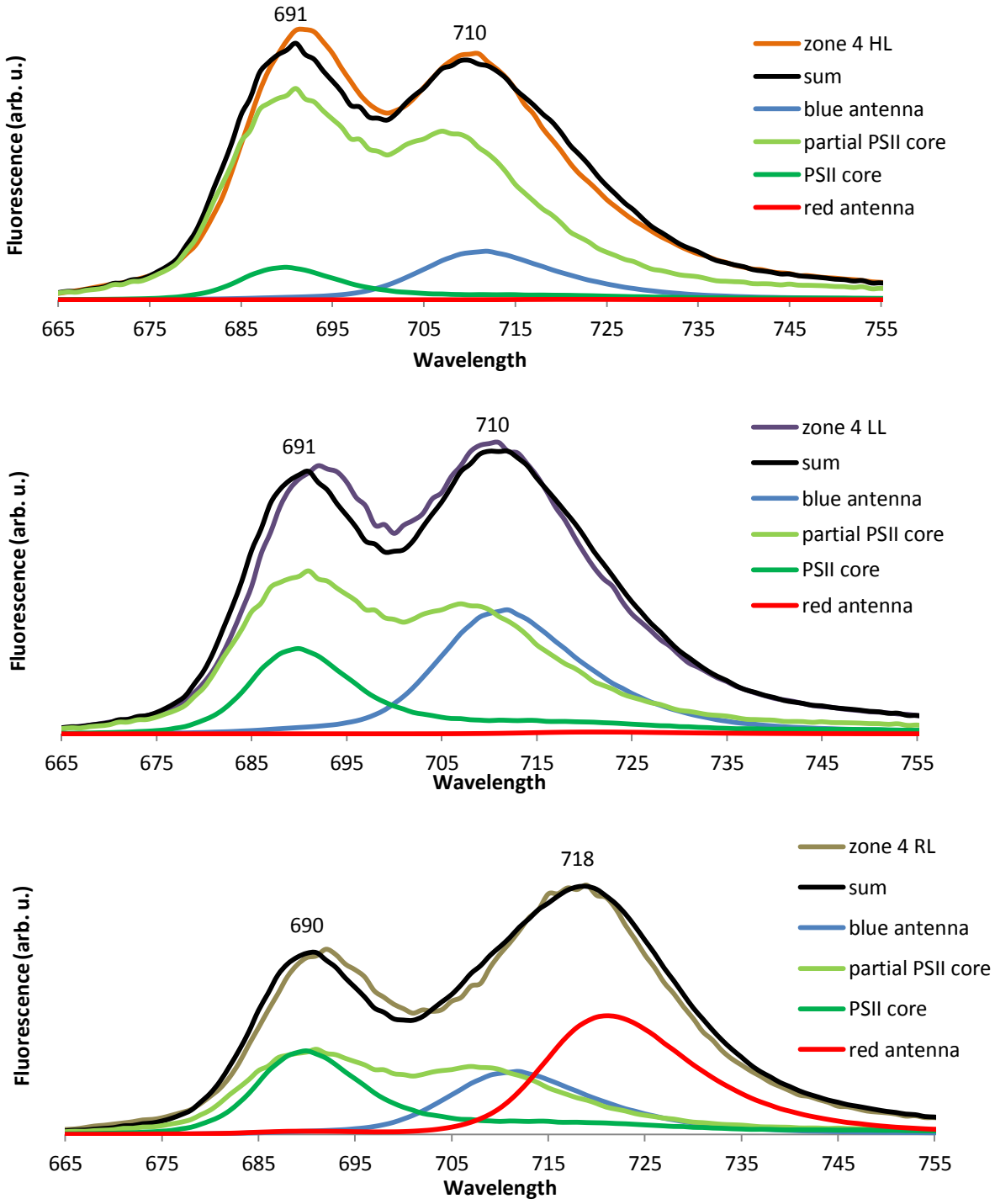

Fig. 33. Analysis and comparison of the probable composition of zone 4 among the three cell variants (HL, LL and RL). Fluorescence 77 K spectra of zone 4 from figure 32 were used as base for the fittings. Spectra of the fitted complexes are taken from CN fluorescence (figure 30). Blue antenna is fraction F4, red antenna represents fractions F6, F8 and F9, PSII core is fraction F7 and partial PSII core is fraction F5 in figure 29.

From these fittings it was deduced, that the difference in RL maximum in figure 32 is caused by presence of the red antenna fluorescence, as shown in figure 33 (bottom). Therefore the cause of chromatic adaptation in *T. minutus* was judged to be this antenna in its various oligomeric stages (F9, F8 and F6, figure 29). To elucidate the possible role of LHC-R protein (identified in figure 27) in the red F9, F8 and F6 antenna complexes, ion exchange chromatography was employed on these gradient zones (section 3.2.3).

Zone 4 from the sucrose gradients, which was analyzed above did not contain any PSI. PSI was found lower in the gradient, due to its bigger size. Fractions F10 and F11 (fig. 29) had very similar fluorescence (figure 34) but F11 is larger according to the CN. The 2D SDS-PAGE (fig. 31) identified F10 as PSI, judging from the similar fluorescence spectra and larger size of F11, F11 was probably PSI with more connected antennas.

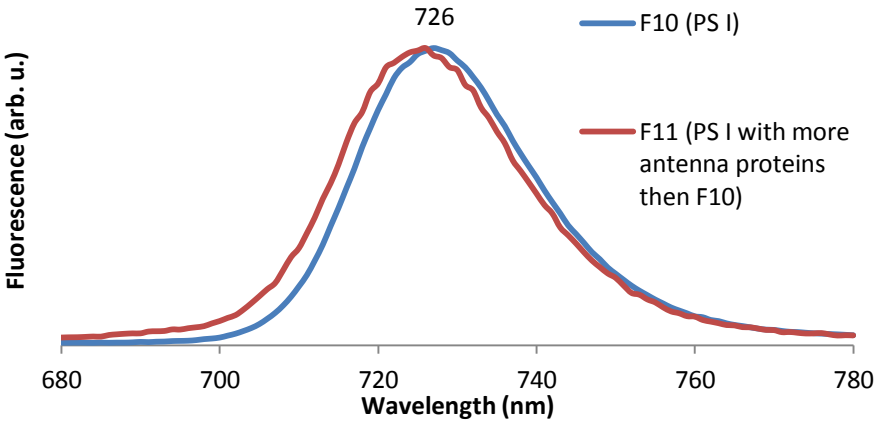

Fig. 34. Fluorescence emission spectra at 77 K of components (F10 and F11, fig. 29.).

3.2.3 Ion exchange chromatography

Fluorescence comparison of gradient zones obtained from RL and LL grown samples showed difference only in zones 3b and 4 (figure 28). An increased presence of one polypeptide, in RL sample, here called LHC-R, was found in those two zones using SDS-PAGE (figure 27). Results from the section 3.2.2 suggest that the presence of large antenna systems is responsible for the fluorescence difference. To investigate the role of LHC-R in these large antennas, ion exchange chromatography was used on zones 3 and 4 of RL sample, where both the red shifted complexes (F6, F8 and F9) and more blue antenna F4 were previously found (figure 29).

Zone 3

Two elutes with the highest chlorophyll density from the anionic chromatography of zone 3 using RL sample (fig. 29) were selected (denoted as i1 and i2). Their analysis by absorbance, 77 K fluorescence spectra and SDS-PAGE is shown in figure 35. Judging from the polypeptide sizes, both fractions are composed of LHC antennas. The fluorescence maximum was found to be at 711 nm, which corresponds with fraction F4 (fig. 29). The relative presence of polypeptide LHC-R compared to the other two LHC polypeptides is low.

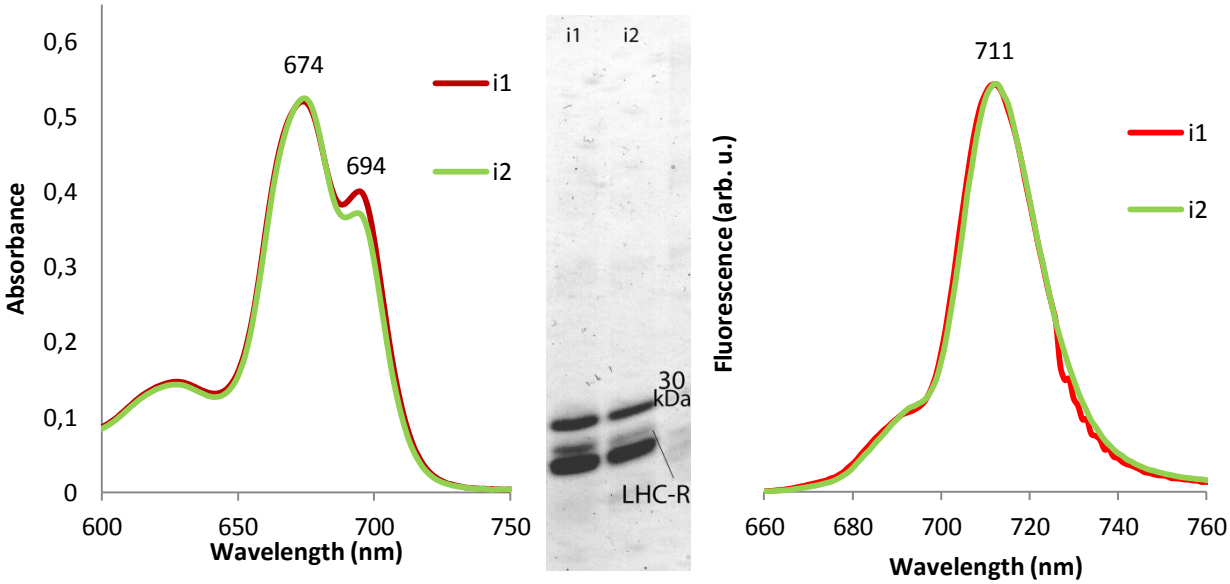

Fig. 35. Room temperature absorbance (left), polypeptide composition (middle) and fluorescence spectrum at 77 K (right) of the selected elutes from ionex chromatography of sucrose gradient zone 3 from RL sample (fig. 29).

Zone 4

Three elutes with the highest chlorophyll density from the anionic chromatography of sucrose gradient zone 4 using RL sample (fig. 29) were selected for analysis (denoted as m1, m2 and m3). Their absorbance and 77 K fluorescence spectra were measured and with electrophoretic analysis are shown in figures 36 and 37.

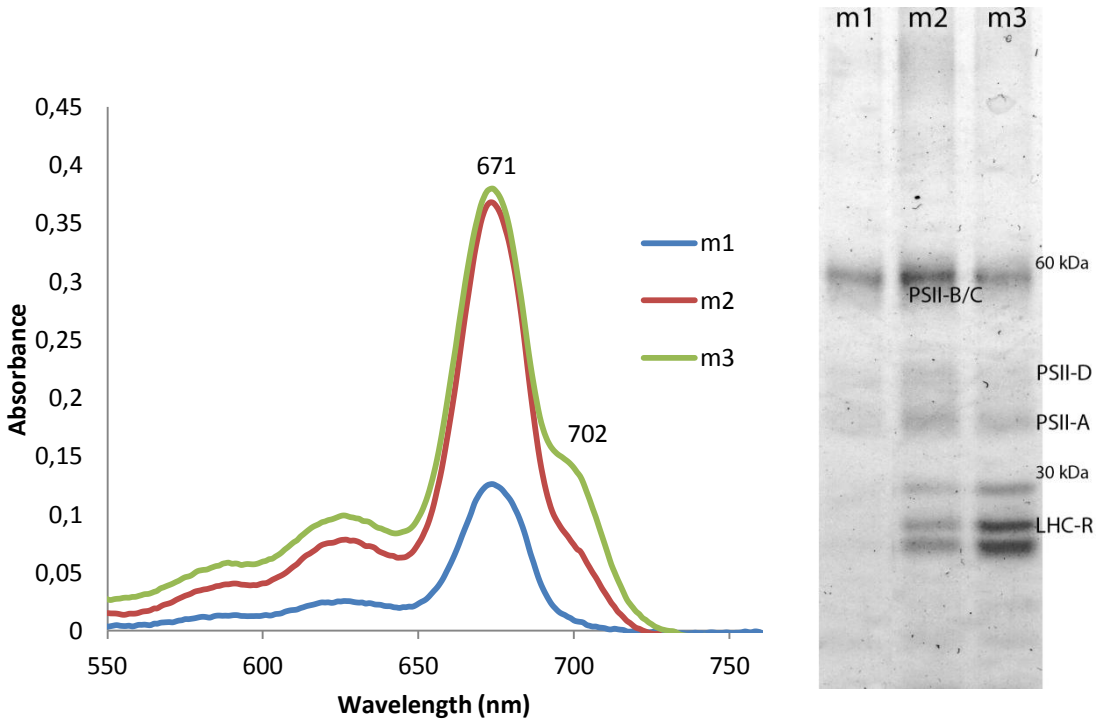

Fig. 36. Absorbance and SDS-PAGE of anionic chromatography fractions m1-m3 from the zone z4 of RL gradient (figure 29).

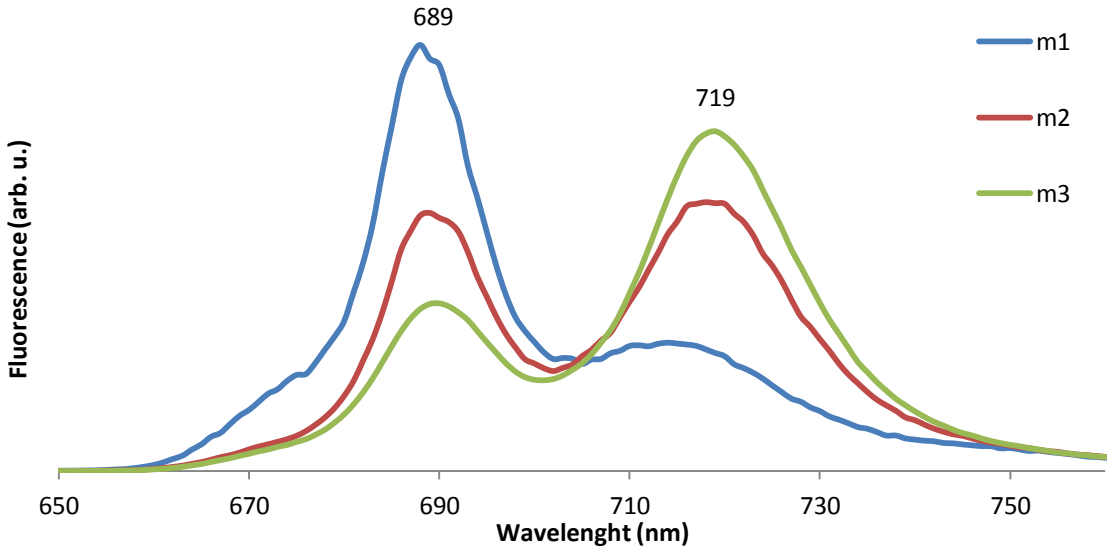

Fig. 37. Fluorescence spectra at 77 K of anionic chromatography fractions m1-m3 from the zone z4 of sucrose RL gradient (figure 29), (for protein composition see fig. 36). The 689 nm maximum corresponds to the core of PSII. The peak at 719 nm corresponds to the LHC oligomers (F6, F8 and F9, figure 29).

Judging from the polypeptide sizes, all three fractions m1, m2 and m3 contain PSII and antennas (fig. 36). As the relative presence of antenna towards PSII increased, an absorption peak at 702 nm and emission peak at 719 nm (fig 37) was detected, the fluorescence

maximum at 719 nm corresponds to fractions F6, F8 and F9; 689 nm corresponds to F7 (fig. 29). The ratio of LHC-R towards the other two LHC polypeptides is much higher when compared with fractions i1 and i2 of zone 3 (fig. 35), suggesting its involvement in the 702 nm light absorption and 719 nm emission.

The maximum of fluorescence emission in figure 35 (711 nm) exactly matches the fluorescence of fraction F4 (figure 29) and also matches the fluorescence maxima of LHC oligomeric zones from HL samples (figures 18, 22 and 26, 711 nm maxima) and LL sample (figure 28, blue line).

On the other hand, fluorescence maximum in Figure 36 (719 nm, fraction m3) matches the fluorescence of fractions F6, F8 and F9 (figure 29) and also matches the maximum of the LHC oligomeric zone 4 from RL sample (figure 28, red line).

Comparing the protein composition of fraction i1, i2, m2 and m3 (figures 35 and 36), the amount LHC-R gets significantly larger in the m2 and m3 fractions relative to the other two LHC sized peptides than in figure 35. These results show that LHC-R must be involved in the spectroscopic difference between the F4 antenna complex and the larger ones (F6, F8 and F9, figure 29).

4. Discussion

The protein and pigment composition of algae antenna systems shows great variability. Understanding this antennae diversity provides information on the connection between their structure, function and adaptation to different environmental factors. In the case of *Trachydiscus* and other algae with a potential for industrial application, detailed knowledge of structure and function of their antenna systems will allow better optimization of their biomass production via genetic engineering.

4.1 Sucrose gradient optimization

Three non-ionic detergents were investigated for the thylakoid membrane solubilization at various concentrations (tab. I), n-dodecyl α-D-maltoside, n-dodecyl β-D-maltoside and digitonin. The effectivity of retaining the protein-pigment complex nativity and their separation on sucrose gradient was compared using fluorescence emission spectra and SDS-PAGE (figures 16-26).

Similar patterns were observed when using the variety of detergents and their concentrations (figures 16-26). In the upper part of the gradient, fluorescence maximum of 680-684 nm was observed belonging to free chlorophyll and partly denatured proteins, corresponding to fraction F1 in CN (fig. 29). The first darker green zone in the gradients always showed emission at 695 nm, belonging to a LHC subunit (possibly a monomer, F2, fig 29). The second dark green zone (poorly resolved in the case of digitonin) had fluorescence maximum at 711-712 nm, which was later found to be an LHC oligomer (F4, fig 29). This result suggests that it is possible to perform the thylakoid membrane solubilization using any of these detergents, when the proper concentration is found.

When using β and α-D-maltoside, a fluorescence maximum of 724 nm was found to dominate in the lower half of the sucrose gradients, belonging to PSI (F10, fig 29). The chosen digitonin concentrations for this work were apparently not sufficient to properly solubilize the thylakoid membranes (no ~724 nm maximum belonging to PSI was observed). Given the molar weight of digitonin being twice as much as D-maltosides (tab. I), the digitonin (m/V)

loads would probably need to be at least twice as large to get comparable results with D-maltosides.

The concentration of β-D-maltoside above 1 % led to bigger dissolution of gradient zone 4, as is apparent from bigger chlorophyll concentration in the upper zones of 2 and 4 % β-DM gradients compared to 0.5 and 1 % (figure 14). This result supports the idea that the zone 4 in figure 14 is in fact made from antenna oligomers, which can dissociate into smaller units upon detergent treatment.

The main difference when using α-D-maltoside compared to the other two detergents was an additional fluorescence maximum at 690 nm (figure 26, lines 4 and 5). It was not observed for the other two detergents in any part of their gradients. Further investigation showed that this maximum belongs to the core of PSII (F7, figures 29, 31). It was possible to make the PSII directly visible on the sucrose gradient by twice freeze thawing the solubilized thylakoid membranes, which resulted in complete breakdown of the larger LHC oligomers. Such sample in the middle part of the gradient lacks LHC oligomers as shown in figure 38. This result suggests that PSII core is much more stable towards repeated freezing and detergent solubilization than the present antenna complexes in *T minutus*.

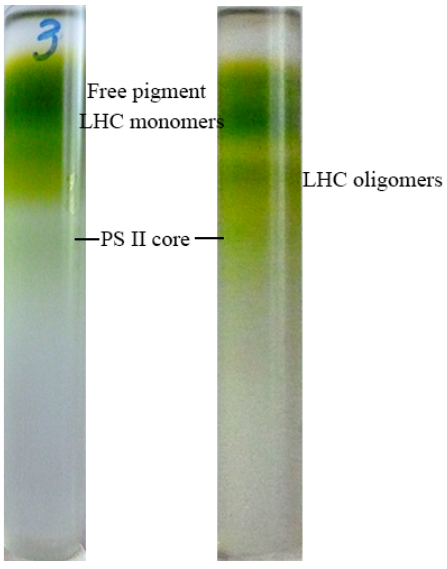

Fig. 38. Comparison of sucrose gradients of freshly solubilized thylakoids (right) and twice freeze-thawed solubilized thylakoids (left), 2,5 % α-DM was used as detergent in both cases. Only the core of PSII remains visible in the middle part of the gradient.

α-D-maltoside was judged to be the better detergent for the analysis than β-DM, because of the presence of PSII core in one zone (zone 4, figure 24, right SDS-PAGE), and containment of the LHC polypeptides to the upper half of the gradient (zones 1-3, figure 24). Similar result was reported by Pagliano *et al.* (2011), when comparing α and β-D-maltoside solubilization

effectivity of large thylakoid complexes, α-D-maltoside was found to retain higher amount of larger complexes compared to its β isoform.

Digitonin gradients (fig. 15) had different profiles than the maltoside gradients, probably because the molecular weight of digitonin is higher (tab. I), thus digitonin forms larger complexes, which are found lower in the sucrose gradients. Also, the various complexes were not as concentrated into distinct bands as in the case of maltosides, Therefore digitonin was not used further.

The sucrose gradient method was also applied on thylakoids isolated from pea (figure 14, left gradient), to get a comparison with higher plants, which were well studied in the past. Similarly looking gradient was also reported by Opačić *et al.* (2014) using *Arabidopsis thaliana*, showing that the sucrose gradient method is well reproducible for various photosynthetic organisms.

Comparison of fluorescence spectra at 295 K and 77 K (figure 20) suggests that low temperature spectra are more effective for identifying various complexes (as used in figure 33) because of their narrower character. Therefore it is also easier to identify whether the signal is coming from one or more complexes, this is especially visible in comparison of zone 2 in figure 20.

4.2 Chromatic adaptation of *T. minutus*

The investigation started by comparing the protein composition and fluorescence properties of RL, LL (figures 27 and 28) and HL sample (figures 24 (2.5 %) and 25). Difference in protein composition was detected in the upper half of the gradient. One protein, here called LHC-R (fig. 27) was significantly more expressed in the RL variant than in LL and HL. LHC-R was detected in the zones 2, 3 and 4. The fluorescence comparison of these three zones showed red shift only in lower part of zone 3 and mainly in the zone 4 as shown on figure 28. This result suggests that the red shift is caused by complex with size similar to PSII, which was also found in the zone 4 of the sucrose gradient. Therefore further focus was primarily to explore the composition of these two zones to a greater detail.

The pigment composition of the RL grown cells was analyzed to be: chlorophyll *a* 54.5 %, violaxanthin 25.9 %, β-carotene 14.1 % and vaucheriaxanthin 5.5 % (R. Litvín, unpublished results). These are the same pigments as reported previously (Přibyl *et al*. 2012) for *T. minutus*. The chromatic adaptation was therefore not caused by synthesis of a pigment with different chemical structure.

4.2.1 Light harvesting complexes found using clean native electrophoresis

To get more detailed information about the composition of the gradient zones from RL sample, which showed new fluorescence maximum at 718 nm (figure 28), which was not detected previously in the high light and low light samples, complexes from the harvested zones were separated using CN (figure 29). Fluorescence 77K emission was measured of the present complexes (figure 30) and to differentiate photosystems from antenna complexes a 2D SDS-PAGE was performed (figure 31).

Even more importantly from the results (figure 29-31) it was possible to assign characteristic fluorescence maximum to each of these complexes, which allowed their identification and relation in all the other fluorescence measurements throughout the thesis. Note that the fluorescence maximum measured from the CN gel is usually 1 or 2 nm shifted to the red compared to fluorescence measured from buffer solutions, which is most likely caused by the different chemical environment of gel and buffer.

Fractions F4, F6, F8 and F9 (figure 29) were judged to be antenna oligomers based on their protein sizes determined by SDS-PAGE (fig. 31). In the CN (fig. 29) these complexes migrated to a position similar to PSII. Since they are all made of proteins with sizes around 20-30 kDa, they had to be oligomers. The ability of Heterokont algae antennas to form oligomers was reported multiple times already, as mentioned in the introduction (Lepetit *et al.* 2012, Basso et al. 2014). These four antenna oligomers (F4, F6, F8 and F9, figure 29) were divided into two groups for further analysis according to their 77 K fluorescence maxima. Three of them show similar fluorescence maximum at ~719 nm (F6, F8 and F9, figure 29) and were called red antenna, and one (F4, fig. 29) has its maximum at 711 nm and was called blue antenna.

The group of three complexes F6, F8 and F9 representing "red antennas" (they probably differ just in the number of subunits, based on the results in section 3.2.3) seem to be responsible for the chromatic adaptation, because they are not dominantly present in HL and LL form (figure 33), and their fluorescence maximum exactly matches the RL sample from figure 28. The fluorescence maximum of the LHC oligomer F4 (fig. 29) at 711 nm is in exact match with fluorescence of LHC zones measured throughout the HL investigation in the section 3.1, and also with the maximum of LL sample on figure 28. This result suggests that complex F4 is the dominant antenna in HL and LL version of the cells.

The complexes F2 and F3 (figure 29) are most likely subunits (monomers or trimers) of the oligomeric antennas mentioned above. F3 showed a local fluorescence maximum at ~715 nm (figure 30), which suggests that it may be a subunit of the F9, F8 and F7 oligomers, with a residual red fluorescence.

Photosystem I was found in the lower half of RL gradient with various amounts of antenna connected (F10, F11, figure 29). This result suggests variable binding strength of PSI antennas towards the core, also that the antennas bind PSI core more tightly than PSII core. PSII was not observed with any peripheral antennas, which is the same result as reported by Basso *et al.* (2014) on *Nannochloropsis gaditana* (also an Eustigmatophyte alga). Photosystem II was found near the middle of the gradient in two main forms, one was probably a monomeric core (F7, fig. 29). The second one was PSII core missing protein PSII-C (F5, figure 31). This result suggests that the PSII-C protein is the weakest bound protein in PSII core, and is the first one to disconnect when detergent solubilization is employed.

When comparing the result for solubilized thylakoids in the CN (figure 29, left side) with the analyzed zones (zones 2-6, right side), it is apparent that no complex was lost during the ultracentrifugation, subsequent zone harvesting and preparation of the zones for the CN. This result suggests that the sucrose gradient method is very effective and correct for separation of protein mixtures with different size. Further, the solubilized thylakoids line, shows much better real proportion between the complexes, as they are inside the thylakoids. This suggests that the antenna fractions F4 and F6 are especially abundant in the RL sample compared to other complexes, especially photosystems. Which implies that during low light conditions the main light absorbing component of thylakoid membranes are antennas.

4.2.2 Mechanism of the chromatic adaptation proposed by fluorescence analysis

After the identification of various complexes present in the sucrose gradient using CN, fluorescence and 2D SDS-PAGE (figures 29, 30 and 31). It was possible to determine the composition of the sucrose gradient zones to a greater detail, as shown in figure 33. It is important to notice that this fitting of different components can be done in multiple ways, all of which would give rather similar sum. However, from the shape of the spectra and their maxima it was possible to determine whether the main contribution is made by a photosystem II or various antennas.

Comparing the fluorescence spectra of HL, LL and RL gradient zones, using α-DM as detergent (figures 26 and 27), the major difference in fluorescence emission was localized to zone 4 and lower part of zone 3. As found in the CN (figure 29) and subsequent analysis (figure 33), the fluorescence shift in zones 3b and 4 was caused by an antenna complex which is dominantly present only in RL version. Analysis in figure 33 also suggests that LL version contains bigger contribution from the blue antenna than HL version, which again supports the theory that the primary antenna function is to provide more energy for reaction centers.

These variable amounts and different kinds of antennas present in HL, LL and RL variants (as shown in figure 33) suggest that *T. minutus* also has a mechanism of regulation of the abundance and character of antennas which get incorporated into its thylakoids, depending on the growth conditions. Same as previously reported for many eukaryotic photosynthetic organisms, for example in chlorophyte alga by Sukenik *et al.* (1988).

4.2.3 Antenna protein composition investigated by ionex chromatography

Second method used to further characterize the zones 3 and 4 (figure 27) of RL sample was separation using anionic chromatography with subsequent absorption and fluorescence measurements and SDS-PAGE analysis of elutes with high chlorophyll concentration. The results of this investigation are depicted on figures 35, 36 and 37.

When fractions i1 and i2 from zone 3 (where the relative amount of LHC-R is low) were compared with fractions m2 and m3 from zone 4 (where the relative amount of LHC-R was higher compared to zone 3), a difference in absorbance was detected. When LHC-R gets

dominant, the red peak on absorption spectrum (fig. 35, 36) shifts from ~694 nm to ~702 nm, which exactly corresponds with the difference in absorbance between RL and HL cells in figure 12, where largely increased absorbance was detected between 700-705 nm. This result suggests that the increased presence of protein LHC-R in antennas was responsible for the chromatic adaptation.

Similarly the fluorescence emission changes (with the increased presence of LHC-R) from 711 nm (fig. 35), which exactly matches the fluorescence of antenna zones detected in HL and LL samples in section 3, to 719 nm, which again matches the maximum fluorescence of zone 4 of RL sample (figure 28). Therefore, from fluorescence spectra it can be also concluded that antenna complexes containing LHC-R protein are directly responsible for the spectroscopic difference depicted in figures 12 and 13.

Based on the chromatography results along with the fluorescence analysis from section 3.2.2, it was concluded that *T. minutus* can build two different types of antennae systems (in figure 33 called red/blue antenna), which differ in the spectral composition of light absorption and fluorescence and also in protein composition. The difference in their 77 K fluorescence maximum is around 10 nm, which could explain the difference depicted in figure 13 (spectra in figure 13 were measured on whole cells).

The elution gradient for anionic exchange chromatography probably could have been chosen less steep, which would possibly result in better separation of the present complexes. However it was possible to determine the role of LHC-R in the chromatic adaptation. Based on the results in section 3.2.3 a theory is proposed, that the red and blue antennas are each made of two apoproteins. They both share one protein (the smallest one in figures 35 and 36). The red shift from blue to red antenna is then caused by switching the other apoprotein (the larger one) for LHC-R. However this could not have been definitely proven. This should be the subject of future investigation.

4.3 Mechanism of the red shift and purpose of the red antenna complexes

Since the pigment analysis did not show any other chlorophyll than chlorophyll *a* (as mentioned earlier in section 4.2), it is reasonable to assume that the increased red light absorption (in RL variant) is absorbed by chlorophyll *a*. Figure 39 shows, that the position of

maximum in the fluorescence emission spectrum corresponds (with the exception of PSII core) to position of the light harvesting complex in the sucrose gradient. With increasing size of each complex the fluorescence of chlorophyll *a* is shifted more towards red, suggesting a connection between the energy of transition and the complex size.

This analysis supports the theory of exciton coupling (van Amerongen *et al*., 2000), where multiple chlorophyll molecules, when close enough and in a favorable orientation to each other, form a intermolecular delocalized HOMO which is, compared to monomers, higher in energy, allowing less energetic transitions, which results in greater absorption of less energetic red light. Therefore it is highly probable that the identified LHC-R protein, by its incorporation into LHC antennas, is bringing multiple chlorophyll molecules in orientations where they can interact with each other more effectively.

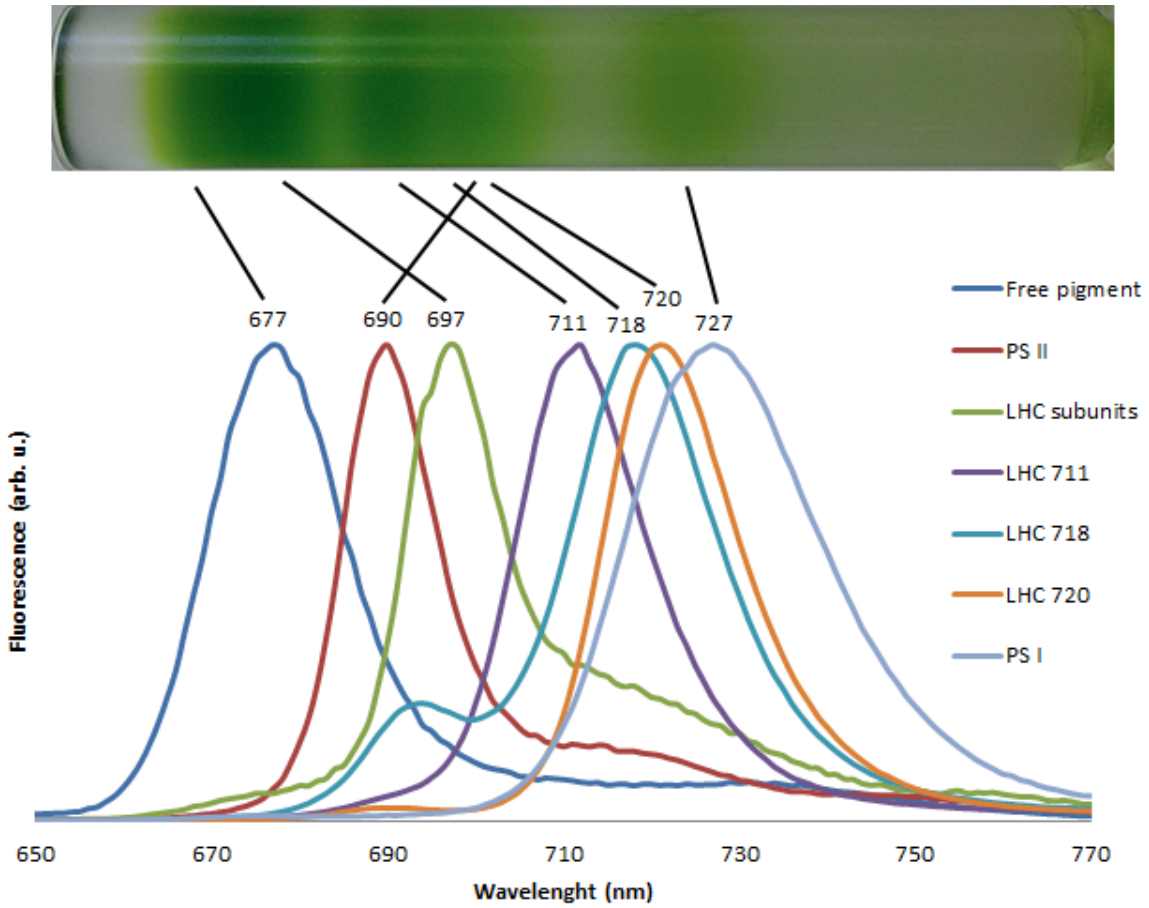

Fig. 39. Comparison of 77 K fluorescence emission maxima with complexes positions in the sucrose gradient, spectra are taken from figure 30 (fraction F4 is here called LHC 711, F6 is LHC 718 and F9 is LHC 720).

The ability of increased light absorption around 700-710 nm (fig. 12) can be an evolutionary advantage for *T. minutus*. As shown in figure 40, around one meter under the water surface containing cyanobacteria, which are omnipresent in our climate, the leftover light is stronger above 700 nm than in between 600-700 nm. Being able to utilize this light effectively enables *T. minutus* to harvest more light than other algae.

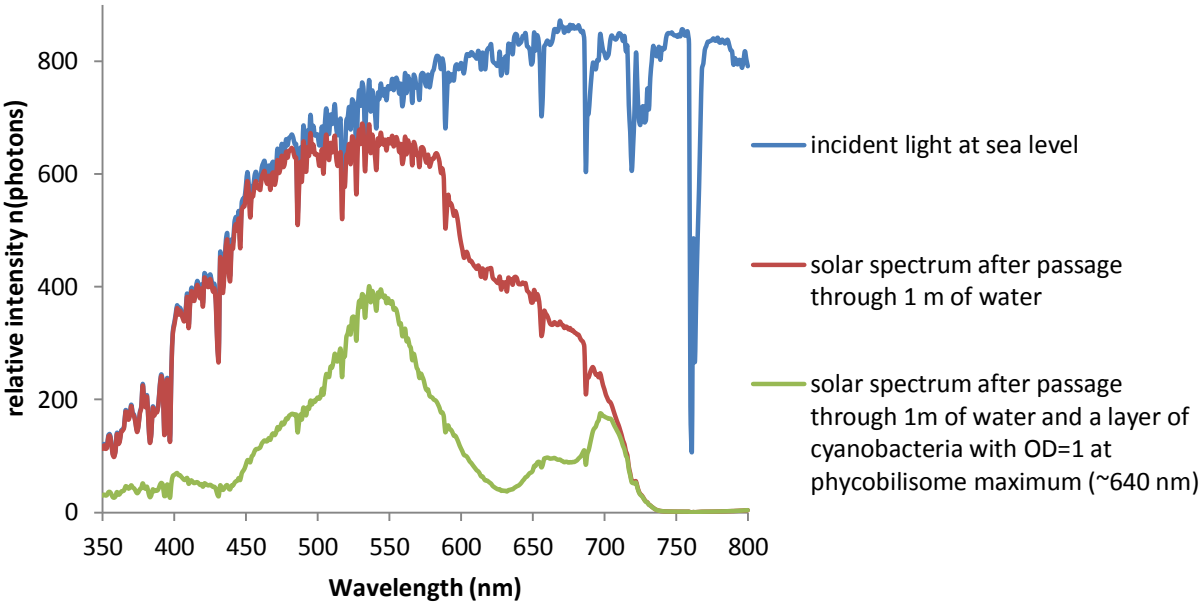

Fig. 40. Model of incident light filtered by cyanobacteria. The peak of available energy above 700 nm is apparent on the green spectrum. Solar spectrum: Sunlight ASTM G173-03 Reference Spectra Derived from SMARTS v. 2.9.2. Water absorption: Buiteveld *et al*. (1994). Cyanobacteria: *Synechococcus* PCC 7002 cells measured locally.

5 Conclusions

- It was determined that n-dodecyl α-D-maltoside provided better separation of *T. minutus* thylakoid membrane components when used as solubilization detergent compared to β-D-maltoside.

- Two major types of light harvesting antennas were found in thylakoids of *T. minutus*. They differ in their light absorption spectra and also in protein composition. Relative quantity of these antennas inside thylakoids changes with variable growth conditions of the cells.

- The chromatic adaptation in *T. minutus* is achieved by increased expression of LHC sized polypeptide (here called LHC-R), which causes creation of large antenna oligomer, which shows fluorescence (77 K) maxima around 720 nm and increased absorption around 702 nm.

- A theory is proposed, that the two identified antenna groups are both made of two apoproteins, while sharing one of them. The nature of the second apoprotein, which in the red antenna is LHC-R, enables the present pigments to utilize less energetic light.

Acknowledgments

This work was supported by GAČR grant 14-01377P. My thanks to Radek Litvín for the thesis supervision and guidance, David Bína for theoretical background and ionex chromatography introduction, Martina Bečková and Zdeno Gardian for clean native electrophoresis presentation, Ivana Hunalová for help with fluorescence measurements, František Matoušek for the thylakoid isolation introduction and Josef Tichý for countless advice during the whole work.

6 References

(1) http://www.chem.qmul.ac.uk/iubmb/enzyme/reaction/polysacc/Calvin2.html

Allen JF (1992) Protein-phosphorylation in regulation of photosynthesis. Biochim. Biophys. Acta, 1098: 275-335.

Arsalane W, Roussea B and Thomas JC (1992) Isolation and characterizazion of native pigment protein complexes from 2 eustigmatophyceae. J. Phycol., 28: 32-36.

Ballottari M, Girardon J, Dall'Osto L and Bassi R (2012) Evolution and functional properties of Photosystem II light harvesting complexes in eukaryotes. Biochimica et Biophysica Acta, 1817: 143-157.

Baniulis D, Yamashita E, Zhang H, et al. (2008) Structure–function of the cytochrome b6 f complex. Photochemistry and Photobiology, 84: 1349–1358.

Basso S, Simionato D, Gerotto C, Segalla A, Giacometti GM and Morosinotto T (2014) Characterization of the photosynthetic apparatus of the Eustigmatophycean *Nannochloropsis gaditana*: Evidence of convergent evolution in the supramolecular organization of photosystem I. Biochimica et Biophysica Acta, 1837: 306-314.

Beer A, Gundermann K, Beckmann J and Büchel C (2006) Subunit composition and pigmentation of fucoxanthin-chlorophyll proteins in diatoms: Evidence for a subunit involved in diadinoxanthin and diatoxanthin binding. Biochemistry, 45: 13046 -13053.

Bína D, Gardian Z, Herbstová M, Kotabová E, Koník P, Litvín R, Prášil O, Tichý J and Vácha F (2014) Novel type of red-shifted chlorophyll a antenna complex from Chromera velia: II. Biochemistry and spectroscopy. Biochimica et Biophysica Acta, 1873: 802-810.

Blankenship RE (2014) Molecular mechanisms of photosynthesis, 2nd edition. Wiley Blackwell, New Jersey.

Buiteveld H, Hakvoort JMH and Donze M (1994) The optical properties of pure water. SPIE Proceedings on Ocean Optics XII, edited by J. S. Jaffe. 2258: 174-183.

C. Büchel (2003) Fucoxanthin-chlorophyll proteins in diatoms: 18 and 19 kDa subunits assemble into different oligomeric states. Biochemistry, 42: 13027–13034.

Calvin M (1989) 40 years of photosynthesis and relatedactivities. Photosynth. Res., 21: 3–16.

Cepák V, Přibyl P, Kohoutková J (2014) Optimization of cultivation conditions for fatty acid composition and EPA production in the eustigmatophycean microalga *Trachydiscus minutus*. J. Appl. Phycol., 26: 181-190.

Dekker JP, Boekema EJ (2005) Supramolecular organization of thylakoid membrane proteins in green plants. Biochimica et Biophysica Acta, 1706: 12-39.

Dekker JP, van Roon H and Boekema EJ (1999) Heptameric association of light- harvesting complex II trimers in partially solubilized photosystem II membranes. FEBS Lett., 449: 211-214.

Fawley KP, Eliáš M and Fawley MW (2014) The diversity and phylogeny of the commercially important algal class Eustigmatophyceae, including the new clade *Goniochloridales*. J. Appl. Phycol., 26: 1773-1782.

Förster T (1965) Delocalized excitation and excitation transfer. In: Modern Quantum Chemistry Istanbul Lectures, Vol. 3 O. Sinanoglu (ed.) New York: Academic Press, pp. 93–137.

Gigova L, Ivanova N, Gacheva G, Andreeva R and Furnadzhieva S (2012) Response of *Trachydiscus minutus* (xanthophyceae) to temperature and light. J. Phycol., 48: 85-93.

Graham JE, Wilcox LW and Graham LE (2008) Algae, 2nd Edn. San Francisco: Benjamin Cummings.

Grouneva I, Rokka A, Eva-Mari A (2011) The Thylakoid Membrane Proteome of Two Marine Diatoms Outlines Both Diatom-Specific and Species-Specific Features of the Photosynthetic Machinery. J. Proteome Res. 10: 5338–5353.

Guillard RRL, Lorenzen CJ (1972) Yellow-green algae with chlorophyllide C. Journal of Phycology, 8: 10-14.

Hasan SS, Yamashita E, Baniulis D and Cramer WA (2013) Quinone-dependent proton transfer pathways in the photosynthetic cytochrome b6f complex. Proc. Natl. Acad. Sci. USA, 110: 4297–4302.

Komenda J, Knoppová J, Kopečná J, Sobotka R, Halada P, Yu J, Nickelsen J, Boehm M and Nixon PJ (2012) The Psb27 assembly factor binds to the CO43 complex of photosystem II in the cyanobacterium Synechocystis sp. PCC 6803. Plant Physiology, 158: 476-486.

Kotabová E, Jarešová J, Kaňa R, Sobotka R, Bína D and Prášil O (2014) Novel type of red-shifted chlorophyll a antenna complex from Chromera velia. I. Physiological relevance and functional connection to photosystems. Biochimica et Biophysica Acta, 1873: 734-743.

Kügler M, Jänsch L, Kruft V, Schmitz UK and Braun HP (1997) Analysis of the chloroplast protein complexes by blue-native polyacrylamide gel electrophoresis (BN-PAGE). Photosynthesis Research, 53: 35-44.

Kühlbrandt W, Wang DN and Fujiyoshi Y (1994) Atomic model of plant light-harvesting complex by electron crystallography. Nature, 367: 614-621.

Laemmli UK (1970) Cleavage of Structural Proteins during the Assembly of the Head of Bacteriophage T4. Nature, 277: 680-685.

Lepetit B, Goss R, Jakob T and Wilhelm C (2012) Molecular dynamics of the diatom thylakoid membrane under different light conditions. Photosynth. Res., 111: 245-257.

Lichtenthaler HK (1987) Chlorophylls and carotenoids - Pigments of photosynthetic biomembranes. Methods in Enzymology, 148: 350-382.

Margulis L (1993) Symbiosis in Cell Evolution: MicrobialCommunities in the Archean and Proterozoic Eons. San Francisco:W. H. Freeman.

Noji H, Yasuda R, Yoshida M and Kinoshita K (1997) Direct observation of the rotation of the F1-ATPase. Nature, 386: 299–302.

Opačić M, Durand G, Bosco M, Polidori A nad Popot JL (2014) Amphipols and Photosynthetic Light-Harvesting Pigment-Protein Complexes. J. Membrane Biol., 247: 1037-1041.

Pagliano C, Barera S, Fabiana C, Saracco G and Barber J (2011) Comparison of the α and β isomeric forms of the detergent n-dodecyl-D-maltoside for solubilizing photosynthetic complexes from pea thylakoid membranes. Biochimica et Biophysica Acta, 1817: 1506-1515.

Pedro AS, González-López CV, Acién FG and Molina-Grima E (2014) Outdoor pilot-scale production of *Nannochloropsis gaditana*: Influence of culture parameters and lipid production rates in tubular photobioreactors. Bioresource Technology, 169: 667-676.

Polivka T and Frank HA (2010) Molecular factors controlling photosynthetic light harvesting by carotenoids. Acc. Chem. Res., 43: 1125–1134.

Přibyl P, Eliáš M, Cepák V, Lukavský J and Kaštánek P (2012) Zoosporogenesis, morphology, ultrastructure, pigment composition, and phylogenetic position of *Trachidiscus minutus* (Eustigmatophyceae, Heterokontophyta). J. Phycol., 48: 231-242.

Řezanka T, Lukavský J, Nedbalová L and Sigler K (2011) Effect of nitrogen and phosphorus starvation on the polyunsaturated triacylglycerol composition, including positional isomer distribution, in the alga *Trachydiscus minutus.* Phytochemistry, 72: 2342-2351.

Řezanka T, Petránková M, Cepák V, Přibyl P, Sigler K and Cajthaml T (2010) *Trachydiscus minutus*, a New Biotechnological Source of Eicosapentaenoic acid. Folia Microbiol., 55: 265-269.

Schmid VHR, Cammarata KV, Bruns BU and Schmidt GW (1997) In vitro reconstitution of the photosystem I light-harvesting complex LHCI-730: Heterodimerization is required for antenna pigment organization. Proc. Natl. Acad. Sci. USA, 94: 7667-7672.

Scholes GD (2010) Quantum-coherent electronic energy transfer: Did nature think of it first? J. Phys. Chem. Lett., 1: 2–8.

Sukenik A, Bennett J, Falkowski P (1998) Changes in the abundance of individual apoproteins of light-harvesting chlorophyll complexes of Photosystem I and II with growth irradiance in the marine chlorophyte Dunaliella tertiolecta. Biochimica et Biophysica Acta, 932: 206-215.

Umena Y, Kawakami K, Shen J and Kamiya N (2011) Crystal structure of oxygen-evolving photosystem II at a resolution of 1.9 Å. Nature, 473: 55-60.

van Amerongen H, van Grondelle R and Valkunas L (2000) Photosynthetic Excitons. London: World Scientific.

Vinyard DJ, Ananyev GM and Dismukes GC (2013) Photosystem II: The Reaction Center of Oxygenic Photosynthesis. Annual Review of Biochemistry, 82: 577–606.

Wientjes E, Oostergetel GT, Jansson S, Boekema EJ and Croce R (2009) The Role of Lhca Complexes in the Supramolecular Organization of Higher Plant Photosystem I. J. Biol. Chem., 284: 7803-7810.

Wientjes E, van Amerongen H and Croce R (2013) LHCII is an antenna of both photosystems after long-term acclimation. Biochimica et Biophysica Acta, 1827: 420-426.

Zhang D, Xue S, Sun Z, Liang K, Wang L, Zhang Q and Cong W (2014) Investigation of continuous-batch mode of two-stage culture of *Nannochloropsis* sp. for lipid production. Bioprocess Biosyst. Eng., 37: 2073-2082.